



ARISTOTLE UNIVERSITY
of THESSALONIKI

Department of Theoretical Physics

THES-TP 96/12

November 1996

PM/96-38



UNIVERSITE MONTPELLIER II
Laboratoire de Physique Mathématique

A Model-independent Description of New Physics effects in $e^+e^- \rightarrow t\bar{t}$ ¹

G.J. Gounaris^a, J. Layssac^b and F.M. Renard^b

^aDepartment of Theoretical Physics, University of Thessaloniki,
Gr-54006, Thessaloniki, Greece.

^bPhysique Mathématique et Théorique, UPRES-A 5032
Université Montpellier II, F-34095 Montpellier Cedex 5.

Abstract

We study the potential of a future e^+e^- collider for the search of anomalous $\gamma t\bar{t}$ and $Zt\bar{t}$ couplings, assuming that CP-invariance holds. This is done in a model-independent way, considering that all six possible couplings do appear. Two experimental situations are envisaged, with and without e^\pm beam polarization. Observability limits in the form of domains in the 6-dimensional parameter space are established. Illustrations for specific constrained models are also presented and implications for new physics searches are discussed.

¹Partially supported by the EC contract CHRX-CT94-0579.

1 Introduction

The properties of the recently discovered top quark [1] has been the subject of many speculations [2]. Theoretical motivations for them deal with the problems of the scalar sector associated to mass generation and the high value of the top mass, close to the value of the electroweak scale. Some experimental hints also came from possible anomalies observed in the heavy quark production at LEP1/SLC [3].

The phenomenological description of non-standard top quark properties mostly rely on the effective lagrangian method which is the proper way to describe New Physics (NP) in case all new degrees of freedom are too heavy to be directly produced in the various Colliders [4]. This effective lagrangian is supposed to be derived from a more fundamental interaction after integrating out the heavy NP degrees of freedom. It describes the residual NP effects in terms of operators involving the Z , W , γ , t , b and gluon fields, with the option of including [5, 6, 7] or not the Higgs boson as a fundamental particle [8].

This way one predicts anomalous properties for the top quark; *i.e.* departures from the Standard Model (SM) couplings that could be revealed by studies of the production and decay modes. Assuming that NP is CP invariant, the set of operators used to construct the effective lagrangian, although restricted by dimensional and gauge symmetry considerations, is rather large, which means a large number of unknown couplings. An underlying theory [9, 10, 11] would certainly relate these couplings to more fundamental parameters. But nowadays such relations are lacking so that studies of NP effects predicted by this description usually proceed by taking each operator one by one and ignoring possible correlations.

In this paper we take a somewhat different attitude. Assuming that NP is CP invariant and that its effects on the process $e^-e^+ \rightarrow t\bar{t}$ only arise from modifications of the $\gamma t\bar{t}$ and $Zt\bar{t}$ vertices, we present a fully model independent analysis of this process, keeping as free parameters all six vector, axial and tensor couplings describing these vertices. We establish observability limits in this 6-dimensional parameter space spanned by the departures from SM values of these couplings. This allows us to discuss discovery limits for NP contributions of any structure. We then also give a few simple illustrations for constrained models where a certain number of relations are imposed among the couplings, leaving for example, only four, three, two or even one free parameters.

We illustrate in full detail the case of 1TeV e^+e^- collider and briefly mention how the results change for the cases of 0.5 or 2 TeV colliders. With the foreseen luminosity one expects more than 10^4 $t\bar{t}$ events in this high energy region [12], so that even after taking into account detection efficiencies [13], the basic accuracy in the determination of the NP couplings is still at the few percent level. If the $\gamma t\bar{t}$ and $Zt\bar{t}$ couplings are assumed to be generated from a specific operator then we can translate the sensitivity limits on the above couplings, to bounds on the corresponding NP scale [7, 14].

In establishing the observability limits we emphasize the special role of a set of angular asymmetries which, to first order in the NP couplings, are independent of the top decay properties and depend only on the structure of the relative magnitudes of the spin density matrix elements of the produced t -quark. This allows us to separate the anomalous effects in the production process that we want to study in the present paper, from those the top decay amplitude, which either modify the tWb vertex or open new decay

channels involving *e.g.* Higgs bosons. We find that a study of the top spin density matrix allows to construct 4 different asymmetries when the e^\pm beams are unpolarized, and 7 additional ones when the e^\pm beams are longitudinally polarized. This way we obtain model-independent constraints on two $\gamma t\bar{t}$ and one $Zt\bar{t}$ couplings which do not receive any SM contribution at tree level; (*i.e.* on d_2^V , d_3^V and d_3^Z below). For the determination of the remaining 3 couplings, one more information is needed which should determine their overall scale. For this we use the magnitude of an integrated top quark density matrix element, like *e.g.* the $t\bar{t}$ production cross section. Such a density matrix element though is of course also sensitive to uncertainties on the top quark decay width and branching ratios. We quantitatively discuss these effects, as well as the implications on the measurements of the aforementioned two sets of couplings for the general 6-parameter case and also for the restricted 1-, 2-, 3- and 4- parameter cases.

Finally we discuss the implications that our results could have on the study of the structure of the underlying NP which can most generally be described in terms of a set of $dim = 6$ operators [4, 7].

The organization of the paper is the following. In Section 2, we present the amplitudes, cross sections and asymmetries, and establish their dependencies on the NP couplings. Section 3 is devoted to the derivation of the constraints on the NP the parameters and to an estimate of the experimental accuracies. Applications are then made in Section 4 to the general 6-parameter cases, as well as the 4-, 3-, 2- and 1- parameter cases. Observability domains are given in Figures and Tables. The final discussion is given in Section 5. Appendix A collects the coefficients of the NP couplings controlling the sensitivity of each observable.

2 Observables

The general CP-conserving structure of the $\gamma t\bar{t}$ and $Zt\bar{t}$ vertices is written as¹ [6]

$$-i\epsilon_\mu^V J_V^\mu = -ie_V \epsilon_\mu^V \bar{u}_t(p) [\gamma^\mu d_1^V(q^2) + \gamma^\mu \gamma^5 d_2^V(q^2) + (p-p')^\mu d_3^V(q^2)/m_t] v_{\bar{t}}(p') , \quad (1)$$

where ϵ_μ^V is the polarization of the vector boson $V = \gamma, Z$. The outgoing momenta (p, p') refer to (t, \bar{t}) respectively and satisfy $q \equiv p + p'$. The normalizations are determined by $e_\gamma \equiv e$ and $e_Z \equiv e/(2s_W c_W)$, while d_i^V are in general q^2 dependent form factors. Non-vanishing contributions to the these couplings from SM at tree level only arise for

$$d_1^{V,SM0} = \frac{2}{3} , \quad d_1^{Z,SM0} = g_{Vt} = \frac{1}{2} - \frac{4}{3}s_W^2 , \quad d_2^{Z,SM0} = -g_{At} = -\frac{1}{2} . \quad (2)$$

Departures from the SM values are then defined as:

$$\bar{d}_j^V \equiv d_j^V - d_j^{V,SM} , \quad (3)$$

¹The definition of d_3^V in (1) differs from the one in [6] by a factor of $1/m_t$.

for $V = \gamma, Z$. The $e^-e^+ \rightarrow t\bar{t}$ helicity amplitude is written as $F_{\lambda,\tau,\tau'}$, where $\lambda \equiv \lambda(e^-) = -\lambda'(e^+) = \pm 1/2$ denote the e^- , e^+ helicities, while τ and τ' represent respectively the t and \bar{t} helicities. Using the couplings defined in (1), we obtain

$$F_{\lambda,\tau,\tau'} = \sum_{V=\gamma,Z} 2\lambda e^2 \sqrt{s} (A_V - 2\lambda B_V) \left\{ d_1^V [2m_t \sin \theta \delta_{\tau\tau'} + \sqrt{s} \cos \theta (\tau' - \tau) - 2\lambda \sqrt{s} \delta_{\tau,-\tau'}] - d_2^V 2|\vec{p}| [\cos \theta \delta_{\tau,-\tau'} + 2\lambda(\tau - \tau')] - d_3^V \frac{4|\vec{p}|^2}{m_t} \sin \theta \delta_{\tau\tau'} \right\}, \quad (4)$$

where A_V, B_V describe the contribution of the vector and axial Vee vertex. In this paper we assume that the Vee vertices are standard, which implies that²

$$A_\gamma = -\frac{1}{s}, \quad A_Z = \frac{g_{Ve}}{4s_W^2 c_W^2 D_Z}, \quad B_\gamma = 0, \quad B_Z = \frac{g_{Ae}}{4s_W^2 c_W^2 D_Z}, \quad (5)$$

$$g_{Ve} = -\frac{1}{2} + 2s_W^2, \quad g_{Ae} = -1/2, \quad (6)$$

and $D_Z = s - M_Z^2 + iM_Z\Gamma_Z$, $s \equiv q^2$. In (4), θ is the (e^-, t) scattering angle in the (e^-, e^+) c.m. frame. Because of CP invariance, the amplitude in (4) satisfies [15]

$$F_{\lambda,\tau,\tau'} = F_{\lambda,-\tau',-\tau}, \quad (7)$$

and is normalized so that the unpolarized $e^-e^+ \rightarrow t\bar{t}$ differential cross section is given by

$$\frac{d\sigma(e^-e^+ \rightarrow t\bar{t})}{d\cos\theta} = \frac{3\beta_t}{128\pi s} \sum_{\lambda,\tau,\tau'} |F_{\lambda,\tau,\tau'}|^2, \quad (8)$$

where $\beta_t = (1 - \frac{4m_t^2}{s})^{1/2}$ and the colour factor has been included.

The density matrix for top-quark production is

$$\rho_{\tau_1\tau_2}^{L,R} = \sum_{\tau'} F_{\lambda,\tau_1,\tau'} F_{\lambda,\tau_2,\tau'}^*, \quad (9)$$

where L, R correspond respectively to $\lambda \equiv \lambda(e^-) = -\lambda'(e^+) = \mp 1/2$. All density matrix elements are real, so long as the imaginary parts of the $d_j^V(q^2)$ are neglected. Because of (7), there are only six independent such elements, namely $\rho_{++}^{L,R}$, $\rho_{--}^{L,R}$ and $\rho_{+-}^{L,R} = \rho_{-+}^{L,R}$, which can be measured through the top production and decay distributions. Unpolarized e^\mp beams allow to measure only the three $(L+R)$ density matrix elements, whereas the three $(L-R)$ ones require longitudinal e^\pm beam polarization.

The general expression of the differential cross section for $e^+e^- \rightarrow t\bar{t}$ with $t \rightarrow bW \rightarrow b\nu_l$ and longitudinally polarized $[L(R) e^-]$ and $[R(L) e^+]$ beams, is written (compare eq.(B6,B7) of [6]) as

²An NP contribution to the Vee vertex of the type suggested by the Class 3 operators of [7] can be also described by the present formalism, by introducing vector and axial γee form factors through $A_\gamma = -d_{1e}^\gamma/s$ and $B_\gamma = -d_{2e}^\gamma/s$, and correspondingly modifying also g_{Ve}, g_{Ae} .

$$\frac{d\sigma^{L,R}}{d\cos\theta d\varphi_1 d\cos\vartheta_1 d\psi_1 d\cos\theta_l} = \frac{9\beta_t\Gamma(t \rightarrow bW)_{SM}Br(W \rightarrow l\nu)}{(8\pi)^3 s(2M_W^2 + m_t^2)\Gamma_t} \rho_{\tau_1\tau_2}^{L,R} \cdot \mathcal{R}_{\tau_1\tau_2} , \quad (10)$$

where Γ_t is the total top width, $\Gamma(t \rightarrow bW)_{SM}$ describes the SM contribution to $t \rightarrow bW$ and the $Wl\nu_l$ vertex is taken to be standard [7].

In (10) the definition

$$\begin{aligned} \rho_{\tau_1\tau_2}^{L,R} \cdot \mathcal{R}_{\tau_1\tau_2} &= \frac{1}{2} (\rho_{++} + \rho_{--})^{L,R} (\mathcal{R}_{++} + \mathcal{R}_{--}) \\ &+ \frac{1}{2} (\rho_{++} - \rho_{--})^{L,R} (\mathcal{R}_{++} - \mathcal{R}_{--}) + \rho_{+-}^{L,R} (\mathcal{R}_{+-} + \mathcal{R}_{-+}) \end{aligned} \quad (11)$$

is used, where the $\mathcal{R}_{\tau_1\tau_2}$ factors are elements of the top decay matrix introduced in eq.(B9-B11) of ref.[6] and include any possible NP contribution to the $t \rightarrow bW$ decay. The quantities \mathcal{R} and the differential cross section in (10), depend on the three Euler angles $(\varphi_1, \vartheta_1, \psi_1)$ determining the $t \rightarrow bW \rightarrow bl\nu_l$ decay plane in the rest frame of the top, as well as on an additional angle θ_l describing the decay distribution of l within the top decay plane. In [6] it has been shown how appropriate averages over the Euler angles allow to project out quantities proportional to each of the three different ρ -factors given in (11), multiplied by top-decay functions depending on the $t \rightarrow Wb$ decay couplings. These averages allow the construction of three types of observables and are done as follows:

- Type A arises by projecting out the first term in (11) including $(\rho_{++} + \rho_{--})^{L,R}$, which is achieved by integrating eq.(10) over $d\varphi_1 d\cos\vartheta_1 d\psi_1 d\cos\theta_l$. These observables measure the structure of the top production differential cross section, when we sum over the t -polarizations.
- Type H , arising from the second term $(\rho_{++} - \rho_{--})^{L,R}$, is related to the top quark helicity. It is extracted through an integration of eq.(10) using the projector

$$P_H = \cos\psi_1 + r \sin\psi_1 \quad , \quad (12)$$

where the parameter r is a priori free. It is chosen

$$r \equiv \frac{3\pi m_t M_W}{4(m_t^2 - 2M_W^2)} \quad , \quad (13)$$

so that to maximize the statistical significance of the results, by optimizing to the angular dependence of the SM distribution.

- Type T , arising from $\rho_{+-}^{L,R}$, is related to the top quark transverse polarization. It is obtained by integrating (10) using the optimized projector,

$$P_T = \cos\psi_1 \sin\varphi_1 \cos\vartheta_1 - \sin\psi_1 \sin\varphi_1 + r(\sin\psi_1 \cos\varphi_1 \cos\vartheta_1 + \cos\psi_1 \sin\varphi_1) \quad . \quad (14)$$

In each of these cases, various asymmetries with respect to the top production angle θ may be constructed, which allows us to get rid of the top-decay couplings contained in the \mathcal{R} factors in (11). Thus, these asymmetries depend only on the six different ρ elements appearing in (11). To present them, let us first single out more precisely the contents of the three types of ρ terms in (11). Using [6], the $\rho^{L\pm R}$ top density matrix elements are expressed, in terms of the $\gamma t\bar{t}$ and $Z t\bar{t}$ couplings (compare (1))

$$d_i^L = d_i^\gamma + \frac{1 - 2s_W^2}{4s_W^2 c_W^2} \chi d_i^Z, \quad d_i^R = d_i^\gamma - \frac{\chi}{2c_W^2} d_i^Z, \quad (15)$$

where $\chi \equiv s/(s - M_Z^2)$ and the Z width is neglected for $s = q^2 > 4m_t^2$. We thus have

$$(\rho_{++} + \rho_{--})^{L\pm R} = 2e^4 \left[\sin^2 \theta \left(\frac{4m_t^2}{s} \right) A_1^{L\pm R} + (1 + \cos^2 \theta) A_2^{L\pm R} - 4\beta_t \cos \theta A_3^{L\pm R} \right], \quad (16)$$

$$(\rho_{++} - \rho_{--})^{L\pm R} = 4e^4 [(1 + \cos^2 \theta) \beta_t B_1^{L\pm R} - \cos \theta B_2^{L\pm R}], \quad (17)$$

$$\rho_{+-}^{L\pm R} = e^4 \left(\frac{4m_t}{\sqrt{s}} \right) \sin \theta [C_1^{L\pm R} - \cos \theta \beta_t C_2^{L\pm R}], \quad (18)$$

where

$$A_1^{L\pm R} = \left[d_1^L - \frac{2|\vec{p}|^2}{m_t^2} d_3^L \right]^2 \pm \left[d_1^R - \frac{2|\vec{p}|^2}{m_t^2} d_3^R \right]^2, \quad (19)$$

$$B_2^{L\pm R} = A_2^{L\mp R} = [(d_1^L)^2 + \beta_t^2 (d_2^L)^2] \mp [(d_1^R)^2 + \beta_t^2 (d_2^R)^2], \quad (20)$$

$$B_1^{L\pm R} = A_3^{L\mp R} = d_1^L d_2^L \pm d_1^R d_2^R, \quad (21)$$

$$C_1^{L\pm R} = d_1^L \left[d_1^L - \frac{2|\vec{p}|^2}{m_t^2} d_3^L \right] \mp d_1^R \left[d_1^R - \frac{2|\vec{p}|^2}{m_t^2} d_3^R \right], \quad (22)$$

$$C_2^{L\pm R} = d_2^L \left[d_1^L - \frac{2|\vec{p}|^2}{m_t^2} d_3^L \right] \pm d_2^R \left[d_1^R - \frac{2|\vec{p}|^2}{m_t^2} d_3^R \right]. \quad (23)$$

Introducing in analogy to (3), the NP contributions \bar{d}_i^L, \bar{d}_i^R to the couplings defined in (15), and expanding to first order in them, we get

$$A_1^{L\pm R} = (d_{1SM}^L)^2 \pm (d_{1SM}^R)^2 + 2d_{1SM}^L \left(\bar{d}_1^L - \frac{2|\vec{p}|^2}{m_t^2} \bar{d}_3^L \right) \pm 2d_{1SM}^R \left(\bar{d}_1^R - \frac{2|\vec{p}|^2}{m_t^2} \bar{d}_3^R \right), \quad (24)$$

$$B_2^{L\pm R} = A_2^{L\mp R} = (d_{1SM}^L)^2 \mp (d_{1SM}^R)^2 + \beta_t^2 [(d_{2SM}^L)^2 \mp (d_{2SM}^R)^2] + 2d_{1SM}^L \bar{d}_1^L \mp 2d_{1SM}^R \bar{d}_1^R + 2\beta_t^2 [d_{2SM}^L \bar{d}_2^L \mp d_{2SM}^R \bar{d}_2^R], \quad (25)$$

$$B_1^{L\pm R} = A_3^{L\mp R} = d_{1SM}^L d_{2SM}^L \pm d_{1SM}^R d_{2SM}^R + d_{1SM}^L \bar{d}_2^L \pm d_{1SM}^R \bar{d}_2^R + d_{2SM}^L \bar{d}_1^L \pm d_{2SM}^R \bar{d}_1^R, \quad (26)$$

$$C_1^{L\pm R} = (d_{1SM}^L)^2 \mp (d_{1SM}^R)^2$$

$$+2d_{1SM}^L \bar{d}_1^L \mp 2d_{1SM}^R \bar{d}_1^R - \frac{2|\vec{p}|^2}{m_t^2} [d_{1SM}^L \bar{d}_3^L \mp d_{1SM}^R \bar{d}_3^R] , \quad (27)$$

$$\begin{aligned} C_2^{L\pm R} &= d_{1SM}^L d_{2SM}^L \pm d_{1SM}^R d_{2SM}^R - \frac{2|\vec{p}|^2}{m_t^2} [d_{2SM}^L \bar{d}_3^L \pm d_{2SM}^R \bar{d}_3^R] \\ &+ d_{1SM}^L \bar{d}_2^L \pm d_{1SM}^R \bar{d}_2^R + d_{2SM}^L \bar{d}_1^L \pm d_{2SM}^R \bar{d}_1^R . \end{aligned} \quad (28)$$

The angular dependence of each of these ρ elements in (16-18) is determined by linear combinations of terms of the form $(1 + \cos^2 \theta)$, $\sin^2 \theta$, $\cos \theta$, $\sin \theta$ and $\sin \theta \cos \theta$. The aforementioned asymmetries just measure the relative ratios of the coefficients of these terms, in each of the three ρ elements mentioned above. Thus, from the $(\rho_{++} + \rho_{--})^{L\pm R}$ elements in (16), involving six $A_j^{L\pm R}$ terms as coefficients of the $\sin^2 \theta$, $(1 + \cos^2 \theta)$ and $\cos \theta$ angular dependencies, we construct five ratios not depending on the top decay properties. From the $(\rho_{++} - \rho_{--})^{L\pm R}$ elements in (17), containing four $B_j^{L\pm R}$ terms associated to the $(1 + \cos^2 \theta)$ and $\cos \theta$ dependencies, we can construct three such ratios. Finally, from the $\rho_{+-}^{L\pm R}$ elements in (18) and its four $C_j^{L\pm R}$ terms associated to the $\sin \theta$ and $\sin \theta \cos \theta$ angular dependencies, another three ratios are possible. Altogether we thus have 11 ratios that can be measured. This is achieved by constructing 4 asymmetries for unpolarized beams and another 7 for polarized ones. They are asymmetries of A -, H - and T -type mentioned above [6]. Below, we enumerate them:

Unpolarized asymmetries

For unpolarized beams there are two A -type asymmetries possible which test $(\rho_{++} + \rho_{--})^{L+R}$. The forward-backward asymmetry

$$A_{FB} = - \left(\frac{3\beta_t}{2} \right) \frac{A_3^{L+R}}{A_2^{L+R} + \frac{2m_t^2}{s} A_1^{L+R}} , \quad (29)$$

and the edge-central one

$$A_{EC} = \left(\frac{3}{16} \right) \frac{A_2^{L+R} - \frac{4m_t^2}{s} A_1^{L+R}}{A_2^{L+R} + \frac{2m_t^2}{s} A_1^{L+R}} . \quad (30)$$

Moreover, there is the forward-backward asymmetry for $(\rho_{++} - \rho_{--})^{L+R}$

$$H_{FB} = - \left(\frac{3}{8\beta_t} \right) \frac{B_2^{L+R}}{B_1^{L+R}} , \quad (31)$$

and the forward-backward asymmetry for $(\rho_{+-})^{L+R}$

$$T_{FB} = - \left(\frac{4\beta_t}{3\pi} \right) \frac{C_2^{L+R}}{C_1^{L+R}} . \quad (32)$$

Polarized asymmetries

For polarized beams there is the left-right asymmetry for the total cross section which

tests $(\rho_{++} + \rho_{--})^{L,R}$ and gives

$$A_{LR} = \frac{\frac{2m_t^2}{s}A_1^{L-R} + A_2^{L-R}}{\frac{2m_t^2}{s}A_1^{L+R} + A_2^{L+R}} , \quad (33)$$

the forward-backward asymmetry of $(\rho_{++} + \rho_{--})^{L-R}$

$$A_{FB}^{pol} = - \left(\frac{3\beta_t}{2} \right) \frac{A_3^{L-R}}{A_2^{L-R} + \frac{2m_t^2}{s}A_1^{L-R}} , \quad (34)$$

the edge-central asymmetry of $(\rho_{++} + \rho_{--})^{L-R}$

$$A_{EC}^{pol} = \left(\frac{3}{16} \right) \frac{A_2^{L-R} - \frac{4m_t^2}{s}A_1^{L-R}}{A_2^{L-R} + \frac{2m_t^2}{s}A_1^{L-R}} . \quad (35)$$

In addition there are two H-type asymmetries which test the left-right asymmetry of $(\rho_{++} - \rho_{--})^{L,R}$ integrated over the t production angle θ

$$H_{LR} = \frac{B_1^{L-R}}{B_1^{L+R}} , \quad (36)$$

and the forward-backward asymmetry of $(\rho_{++} - \rho_{--})^{L-R}$

$$H_{FB}^{pol} = - \left(\frac{3}{8\beta_t} \right) \frac{B_2^{L-R}}{B_1^{L-R}} , \quad (37)$$

and another two T-type asymmetries testing the left-right asymmetry of the integrated $(\rho_{+-})^{L,R}$

$$T_{LR} = \frac{C_1^{L-R}}{C_1^{L+R}} , \quad (38)$$

and the forward-backward asymmetry of $(\rho_{+-})^{L-R}$

$$T_{FB}^{pol} = - \left(\frac{4\beta_t}{3\pi} \right) \frac{C_2^{L-R}}{C_1^{L-R}} . \quad (39)$$

To these 11 asymmetries which are independent of any NP effects in the top decay couplings, we now add the three quantities measuring the overall magnitude of the unpolarized ρ^{L+R} elements in (11), integrated over θ . These elements, multiplied by $Br(t \rightarrow bW \rightarrow bl\nu_l)$, are obtained from the event distribution (10), either by simply integrating over the Euler angles of the top decay plane, or by also using the projectors mentioned (12, 14) [6].

For determining the overall magnitude of the ρ 's, the knowledge of $Br(t \rightarrow bW \rightarrow bl\nu_l)$ is needed. Thus, integrating (10) and dividing the result by $Br(t \rightarrow bW \rightarrow bl\nu_l)$, we get the unpolarized $e^-e^+ \rightarrow t\bar{t}$ total cross section

$$\sigma_t = \sigma(e^-e^+ \rightarrow t\bar{t}) = \frac{\int d\sigma^{L+R}}{Br(t \rightarrow bW \rightarrow bl\nu_l)} = \frac{2\pi\alpha^2\beta_t}{s} \left[\frac{2m_t^2}{s}A_1^{L+R} + A_2^{L+R} \right] , \quad (40)$$

determined by $(\rho_{++} + \rho_{--})^{L+R}$ in (16). The quantity σ_t is of course a type A observable, according to the above classification. We also have the type H observable determined by $(\rho_{++} - \rho_{--})^{L+R}$ in (17) and defined by

$$H_t = \frac{\int P_H d\sigma^{L+R}}{Br(t \rightarrow bW \rightarrow bl\nu_l)} = \frac{\pi^2 \beta_t^2 \alpha^2 (m_t^2 - 2M_W^2)(1+r^2)}{2s(m_t^2 + 2M_W^2)} B_1^{L+R} , \quad (41)$$

in terms of the projector in (12) and $d\sigma^{L+R}$ from (10). Finally $(\rho_{+-})^{L+R}$ in (18) determines T_t through

$$T_t = \frac{\int P_T d\sigma^{L+R}}{Br(t \rightarrow bW \rightarrow bl\nu_l)} = \frac{\pi^2 \beta_t \alpha^2 m_t (m_t^2 - 2M_W^2)(1+r^2)}{2s^{3/2}(m_t^2 + 2M_W^2)} C_1^{L+R} , \quad (42)$$

using the projector in (14) and r given in eq.(13). The effect on these quantities, of the top decay branching ratio and of the detection efficiencies, will be taken into account in Section 3.

So in the whole, we have the 14 observables in (29-42) corresponding to the measurements of the coefficients of the various angular terms appearing in the ρ elements. Eleven of these observables, defined in (29-39), are ratios of such coefficients, which are therefore independent of the top-decay parameters involving the 10 combinations of couplings defined in (19-23) or (24-28) .

3 Experimental accuracies and constraints

The analysis then proceeds by writing for each of the 14 observables \mathcal{A}^i in (29- 42), the departures from the SM prediction at first order in NP parameters, as

$$\delta\mathcal{A}^i \equiv \mathcal{A}^i - \mathcal{A}^{i,SM} = \sum_{j=1,6} K_j^i \bar{d}_j . \quad (43)$$

The coefficients K_j^i , deduced from the expansions (24-28), are given in Appendix A.

A priori it could seem sufficient to just use the 11 asymmetries for a determination of the six NP couplings, since the asymmetries are experimentally preferable quantities being independent of the overall normalization of the data. But this is actually not true, since asymmetries are only sensitive to the relative ratios of the d_j^Z , d_j^γ ($j = 1 - 3$) couplings. Thus, asymmetries cannot impose important constraints on couplings receiving non-vanishing values in SM at tree level. Additional information is needed to fix the overall normalization of these couplings. This can either be done by using an extra measurement sensitive to overall coupling normalization, or by imposing an appropriate non-homogeneous constraint which will force some of the couplings that have non vanishing SM values, to retain their magnitudes even in the presence of NP.

- Thus we can use the measurements of the total $e^+e^- \rightarrow t\bar{t}$ cross section σ_t , and/or any of the two other combinations of the integrated ρ density matrix elements expressed through the quantities H_t or T_t ; compare (40-42). As mentioned previously,

these quantities are sensitive to the top quark decay width. To take this into account we consider two extreme cases for the uncertainties of σ_t , H_t or T_t . In the first case these uncertainties are taken to be $\sim 2\%$, which is of the order of magnitude of possible NP effects in $t \rightarrow Wb$ and the $\gamma t\bar{t}$ or $Zt\bar{t}$ couplings; while in the second case we take the uncertainties to be of order of 20%, which is the type of uncertainty expected for the experimental measurement of the top decay width[13].

- Alternatively, we impose a (non-homogeneous) constraint on the d_j^V , like *e.g.* forcing some of them to have their SM values. For example this is what happens in the 3- or 4-parameter cases presented below.

The observability limits are now obtained by the following procedure. For each observable \mathcal{A}^i , we estimate an experimental uncertainty $\delta\mathcal{A}_{exp}^i$. Following [13], we assume an overall reduction of the number of events by a factor 0.18 due to branching ratios, reconstruction of events, efficiencies and detector acceptance. We then apply statistical considerations to the projected events, in the three types A, H and T observables defined above. The results are given in Table 1.

Assuming that the measurements coincide with the SM expectations and demanding that for an NP effect to be observable, the statistical uncertainty should be smaller than the effect expected due to the NP couplings \bar{d}_j^V (compare 24-28), we write for each observable the inequality

$$\left| \sum_{j=1}^n K_j^i \bar{d}_j \right| \geq \frac{\delta\mathcal{A}_{exp}^i}{\mathcal{A}_{SM}^i} , \quad (44)$$

where $n \leq 6$ NP is the number of the NP couplings considered. We then combine quadratically all such information coming from the l available observables. This gives at one standard deviation the observability domain which is outside the ellipsoid surface

$$\sum_{i=1}^l \left| \sum_{j=1}^n [K_j^i \bar{d}_j] \cdot \left[\frac{\delta\mathcal{A}_{exp}^i}{\mathcal{A}_{SM}^i} \right]^{-1} \right|^2 = 1 \quad (45)$$

4 Applications

4.1 6-parameter case

We first consider the most general case with 6 free parameters $\bar{d}_i^\gamma, \bar{d}_i^Z, i = 1, 2, 3$. Results are collected in Table 2 for a 0.5, 1, 2 TeV collider and illustrated in Fig.1 for the 1 TeV case. Remember that only the three parameters d_1^γ, d_1^Z, d_2^Z receive SM tree level contributions. We start by considering the constraints due to all 11 asymmetries, assuming that polarized e^\pm beams are available. As expected, only the 3 pure NP couplings $\bar{d}_2^\gamma, \bar{d}_3^\gamma, \bar{d}_3^Z$, (for which there is no SM analog), are then strictly constrained, as one can see in Fig.1(d,e,f) and in Table 2. For these three couplings, the observability limit is around

$$|\bar{d}_j| \gtrsim 0.01 . \quad (46)$$

Among the other 3 couplings, \bar{d}_1^γ , \bar{d}_1^Z , \bar{d}_2^Z , one constraint is missing and this is the origin of the band in Figs.1a,c,e relating pairs of these parameters. The width of the band is of a few percent.

We have then considered how a measurement of σ_t , H_t and T_t with an uncertainty of 20% or 2% on the decay width would limit these bands. In fact only one of these quantities would be sufficient to limit the bands, and it turns out that σ_t is the most efficient, since the statistical weight associated to it is the largest. In the following results all three informations are statistically included in the ellipsoid. This is also shown in Fig.1a,c,e where one sees that the band is transformed into ellipses whose sizes are of the order of ± 0.025 to 0.05. In addition in Table 2 and in Fig.1(g,i,k) one sees, as expected, that this additional information does not much improve the determination of the set of three pure NP couplings which are already severely constrained by the asymmetries.

If no e^\pm beam polarization is available, we have only 4 asymmetries at our disposal, and it is necessary to add the information coming from σ_t , H_t , T_t in order to constrain the system of 6 free parameters. The results are shown in Table 3 and in Fig.1(b,d,f,h,j,l). The constraints on the pure NP couplings \bar{d}_2^γ , \bar{d}_3^γ , \bar{d}_3^Z , are now a factor 2 less stringent; *i.e.* they lie at the 0.02 level. The other three couplings get also more freedom by a factor 2 and are now allowed to reach the 0.08 level.

All our figures correspond to the case of a 1 TeV collider. Expectations for 0.5 TeV and 2 TeV can be compared in Tables 2-7. The change is not dramatic. The most notable energy dependence concerns the tensor couplings d_3^V . For the other ones the sensitivity is much milder. Remember that we assumed that the luminosity grows like s so that the number of events is roughly the same at all three considered energies. So only the intrinsic s dependence of the NP couplings shows up in this comparison.

4.2 4-parameter case

We here consider the case of only 4 free parameters. We impose the photon NP couplings to be of a pure $\sigma_{\mu\nu}q^\nu$ type with no axial coupling, that means

$$\bar{d}_1^\gamma = -2\bar{d}_3^\gamma \quad , \quad \bar{d}_2^\gamma = 0 \quad , \quad (47)$$

so that the 4 free parameters are taken as \bar{d}_3^γ and \bar{d}_i^Z ($i = 1, 2, 3$). This constraint is satisfied by the tree level NP contributions of all operators considered in [6]. In the notations of [6], these operators are \mathcal{O}_{t2} , \mathcal{O}_{Dt} , $\mathcal{O}_{tW\Phi}$ and $\mathcal{O}_{tB\Phi}$.

We have considered both polarized (11 asymmetries) and unpolarized (4 asymmetries) cases, illustrated in Fig.2 (a,c,e,g,i,k) and (b,d,f,h,j,l), respectively. We observe that a meaningful constraint is already obtained in the unpolarized case at the 0.1 level without σ_t , H_t or T_t measurements. Furthermore, in this case the additional constraint due to a measurement of σ_t at a 20 % accuracy, reduces the allowed domain by a factor 5, while another factor 2 would be obtained if the accuracy is at 2%. Having polarized observables at our disposal improves notably the constraints, reaching the 0.01 level, even when only asymmetries are used; compare Fig.2 and Table 4.

4.3 3-parameter case

A 3-parameter case is obtained from the 4-parameter one by imposing that the NP contribution to the $Zt\bar{t}$ couplings only involves the $\sigma^{\mu\nu}q_\nu$ and the right-handed $\gamma^\mu(1 + \gamma^5)$ couplings. This is suggested by the tree level contributions of the dynamical models studied in [10]. Indeed, it has been found that in the dynamical models studied in [10], that only three operators can be generated which contribute at tree level to the $Zt\bar{t}$ vertex. These operators, named \mathcal{O}_{t2} , $\mathcal{O}_{tW\Phi}$ and $\mathcal{O}_{tB\Phi}$ in [10], lead precisely to the aforementioned types of couplings.

We first show in Fig.3 the ellipsoid containing the invisible domain at 1 TeV in the 3-parameter space $(\bar{d}_3^Z, \bar{d}_2^Z, \bar{d}_3^Z)$, for the polarized case. When projected on the three axes one obtains the ellipses shown in Fig.4(a,c,e). The comparison with the unpolarized case is done with Fig.4(b,d,f). Results for these NP couplings, collected in Table 5, appear to be of similar type as those of the 4-parameter case, with the constraints reduced by roughly a factor 2. In some cases these constraints reach the 0.005 level.

4.4 2-parameter case

We have also analyzed the 2-parameter case suggested by the chiral description. In this case NP contribute only to the vector and axial couplings of the Z. The effective Lagrangian is written as [8]

$$\mathcal{L} = -\frac{e}{4s_Wc_W}\bar{\Psi}_t[\kappa_L^{NC}\gamma^\mu(1 - \gamma^5) + \kappa_R^{NC}\gamma^\mu(1 + \gamma^5)]\Psi_t Z_\mu \quad , \quad (48)$$

which gives the NP contributions in our notations as:

$$\bar{d}_1^Z = \frac{1}{2}[\kappa_L^{NC} + \kappa_R^{NC} - (1 - \frac{8}{3}s_W^2)] \quad , \quad (49)$$

$$\bar{d}_2^Z = -\frac{1}{2}[\kappa_L^{NC} - \kappa_R^{NC} - 1] \quad . \quad (50)$$

The corresponding constraints are shown in Fig.5 and Table 6. One can appreciate the role of the polarization (an improvement from the 0.1 to the 0.01–0.02 level). Also in the unpolarized case the measurement of the cross section allows to reach the few 0.01 level, but with polarization this level is already obtained with asymmetries only.

4.5 1-parameter case

Finally we reconsider the simplest case in which all effective operators listed in [6] are taken one by one. We want to appreciate the role of the different observables in obtaining the constraints on the associated coupling constants. The expressions of the \bar{d}_j couplings have been established in [6]. Results are given in Table 7 for the polarized and the unpolarized case. Corresponding to each coupling we give in parenthesis the value of the NP scale obtained from the unitarity relations established in [7]. The values are in the

order of magnitude expected from the rough analysis made in [6]. Polarization generally increases the visibility domain by a factor 2. Operators contributing at tree level lead obviously to the largest effects and in some cases NP scales of the order of 50 TeV can be reached.

5 Conclusions

In this paper we have studied the observability of NP effects on the $\gamma t\bar{t}$ and $Zt\bar{t}$ couplings in a model independent way through the process $e^-e^+ \rightarrow t\bar{t}$. We have considered the rather general situation involving the 6 anomalous CP-conserving couplings.

We have first tried an analysis which would not be affected by the unknown top quark decay couplings. For that purpose we have used 4 unpolarized and 7 polarized asymmetries, constructed from the top quark density matrix elements, which are independent of the decay couplings. We have obtained severe constraints on the set of the 3 pure NP couplings; *i.e.* those that receive no SM contributions. The observability limits in this set of NP couplings (d_2^V , d_3^V and d_3^Z) vary from 0.01 to 0.02, independently of any top decay uncertainties.

For the other three couplings d_1^V , d_1^Z and d_2^Z , which receive tree level SM contributions, asymmetries are not sufficient to constrain them and one additional information is needed. We have thus added the informations coming from the integrated top density matrix elements and discussed the influence of the uncertainty affecting the top decay width. Varying it from 2% to 20%, the observability limits for this set of couplings lie in the range 0.01 to 0.05.

The improvement brought by e^\pm beam polarization corresponds to roughly a reduction of the invisible domain by a factor 2.

We have also considered 3 different e^+e^- collider energies, 0.5, 1 and 2 TeV. The order of magnitude of the observability limits for \bar{d}_1 and \bar{d}_2 , do not depend strongly on the energy. On the contrary, for the tensor coupling \bar{d}_3 , the sensitivity increases by one order of magnitude, as the energy increases from 0.5 to 2TeV.

We have also considered more specific cases of NP models in which the number of free parameters is reduced. In these cases asymmetries alone allow to constrain all parameters, because there exist relations between the two aforementioned sets of NP couplings. In such cases, it is possible to get strong constraints that are independent of the top decay couplings. We have made illustrations for the case of 4-parameter, 3-parameter, 2-parameter and 1-parameter models, suggested by the effective lagrangian descriptions. Visibility domains are obviously now increased, reaching in some cases the few permille level. As compared to present indirect constraints from LEP/SLC (which are at the 10% level in the 2-parameter case) [16], and to the constraints expected on the charged current couplings Wtb at LHC (also at the 10% level) [8], this represents an important improvement.

Translating to NP scales through the unitarity relations [7, 14], we find that the percent level in the sensitivity to these couplings (precise values depending on the considered

operators), corresponds to NP scales in the 10 TeV region.

Finally we should state that our analysis is of theoretical nature and should certainly be adapted to specific experimental and detection configurations. We believe though, that it has the advantage of pointing out the merit of each type of observable, and of specifying the results which do not depend on assumptions about the possibly unknown top decay couplings.

Table 1: Expected accuracy on observables

	Integrated ρ -elements		
Norm. accuracy	$\delta\sigma_t/\sigma_t$	$\delta H_t/H_t$	$\delta T_t/T_t$
$\delta\Gamma_t/\Gamma_t = 0.02$	0.028	0.19	0.29
$\delta\Gamma_t/\Gamma_t = 0.20$	0.20	0.27	0.35

Unpolarized Asymmetries				Polarized Asymmetries						
δA_{FB}	δA_{EC}	δH_{FB}	δT_{FB}	$\delta A_{LR}^{(A)}$	$\delta A_{FB}^{(pol)}$	$\delta A_{EC}^{(pol)}$	$\delta A_{LR}^{(B)}$	$\delta H_{FB}^{(pol)}$	$\delta A_{LR}^{(C)}$	δT_{FB}^{pol}
0.017	0.020	0.23	0.31	0.019	0.050	0.058	0.75	0.053	0.82	0.11

Table 2: Sensitivity limits for 6 free parameters in the polarized case

(For each energy the three lines correspond to constraints obtained, without (σ_t, H_t, T_t) , or with σ_t, H_t, T_t , assuming a normalization uncertainty of 2% or 20%)

\sqrt{s}	$\delta\Gamma_t/\Gamma_t$	\bar{d}_1^γ	\bar{d}_2^γ	\bar{d}_3^γ	\bar{d}_1^Z	\bar{d}_2^Z	\bar{d}_3^Z
0.5	no σ_t, H_t, T_t	—	0.020	0.049	—	—	0.050
0.5	20%	0.055	0.019	0.043	0.032	0.049	0.044
0.5	2%	0.023	0.018	0.043	0.026	0.031	0.039
1	no σ_t, H_t, T_t	—	0.014	0.016	—	—	0.010
1	20%	0.056	0.013	0.014	0.025	0.044	0.008
1	2%	0.019	0.013	0.014	0.018	0.022	0.007
2	no σ_t, H_t, T_t	—	0.013	0.012	—	—	0.006
2	20%	0.056	0.012	0.008	0.023	0.044	0.003
2	2%	0.016	0.011	0.008	0.016	0.020	0.003

Table 3: Sensitivity limits for 6 free parameters in the unpolarized case
(with σ_t, H_t, T_t and a 2% or 20% normalization uncertainty)

\sqrt{s}	$\delta\Gamma_t/\Gamma_t$	\bar{d}_1^γ	\bar{d}_2^γ	\bar{d}_3^γ	\bar{d}_1^Z	\bar{d}_2^Z	\bar{d}_3^Z
0.5	20%	0.082	0.032	0.056	0.103	0.063	0.109
0.5	2%	0.034	0.031	0.055	0.093	0.041	0.096
1	20%	0.081	0.024	0.021	0.081	0.057	0.016
1	2%	0.031	0.023	0.021	0.067	0.031	0.014
2	20%	0.081	0.023	0.017	0.078	0.056	0.006
2	2%	0.030	0.022	0.017	0.063	0.030	0.006

Table 4: Sensitivity limits with 4 free parameters
(same captions as in Table 2)

\sqrt{s}	$\delta\Gamma_t/\Gamma_t$	Polarized				Unpolarized			
		\bar{d}_3^γ	\bar{d}_1^Z	\bar{d}_2^Z	\bar{d}_3^Z	\bar{d}_3^γ	\bar{d}_1^Z	\bar{d}_2^Z	\bar{d}_3^Z
0.5	no σ_t, H_t, T_t	0.042	0.040	0.089	0.042	0.140	0.391	0.235	0.693
0.5	20%	0.018	0.026	0.043	0.038	0.006	0.057	0.029	0.070
0.5	2%	0.004	0.020	0.025	0.033	0.006	0.070	0.029	0.071
1	no σ_t, H_t, T_t	0.015	0.020	0.046	0.010	0.030	0.302	0.111	0.123
1	20%	0.010	0.017	0.032	0.007	0.015	0.065	0.041	0.013
1	2%	0.004	0.014	0.017	0.006	0.005	0.048	0.020	0.010
2	no σ_t, H_t, T_t	0.012	0.016	0.041	0.005	0.018	0.291	0.104	0.051
2	20%	0.007	0.014	0.026	0.003	0.004	0.038	0.018	0.004
2	2%	0.003	0.012	0.016	0.003	0.005	0.044	0.018	0.004

Table 5: Sensitivity limits with 3 free parameters
(same captions as in Table 2)

\sqrt{s}	$\delta\Gamma_t/\Gamma_t$	Polarized			Unpolarized		
		\bar{d}_3^{γ}	\bar{d}_2^Z	\bar{d}_3^Z	\bar{d}_3^{γ}	\bar{d}_2^Z	\bar{d}_3^Z
0.5	no σ_t, H_t, T_t	0.026	0.055	0.029	0.048	0.104	0.220
0.5	20%	0.015	0.035	0.017	0.025	0.053	0.021
0.5	2%	0.004	0.024	0.011	0.005	0.029	0.015
1	no σ_t, H_t, T_t	0.009	0.023	0.009	0.023	0.055	0.106
1	20%	0.007	0.017	0.006	0.015	0.038	0.008
1	2%	0.004	0.014	0.005	0.004	0.019	0.007
2	no σ_t, H_t, T_t	0.007	0.015	0.005	0.016	0.043	0.050
2	20%	0.005	0.011	0.003	0.038	0.018	0.004
2	2%	0.003	0.010	0.002	0.013	0.034	0.004

Table 6: Sensitivity limits with 2 free parameters
(same captions as in Table 2)

\sqrt{s}	$\delta\Gamma_t/\Gamma_t$	Polarized		Unpolarized	
		\bar{d}_1^Z	\bar{d}_2^Z	\bar{d}_1^Z	\bar{d}_2^Z
0.5	no σ_t, H_t, T_t	0.012	0.027	0.373	0.090
0.5	20%	0.012	0.027	0.042	0.032
0.5	2%	0.010	0.025	0.026	0.029
1	no σ_t, H_t, T_t	0.012	0.020	0.286	0.074
1	20%	0.012	0.020	0.045	0.024
1	2%	0.011	0.017	0.030	0.020
2	no σ_t, H_t, T_t	0.013	0.019	0.276	0.074
2	20%	0.012	0.019	0.052	0.024
2	2%	0.011	0.016	0.032	0.018

Table 7: Sensitivity limits for 1 free parameter, polarized/unpolarized cases
(Limits correspond to the couplings associated to each operator, the corresponding value of the NP scale is indicated below. The column "other constraints" refers to LEP1/SLC
(a) from ϵ_i , (b) from R_b and (c) to limits expected from LEP2.

Operator	$\sqrt{s} = 0.5$ TeV	$\sqrt{s} = 1$ TeV	$\sqrt{s} = 2$ TeV	other constraints
\mathcal{O}_{qt}	0.53/1.62 (0.98)/(0.56)	0.26/0.53 (1.41)/(0.99)	0.18/0.31 (1.68)/(1.29)	$-0.14 \pm 0.07^{(b)}$
$\mathcal{O}_{qt}^{(8)}$	0.10/0.30 (2.47)/(1.42)	0.049/0.099 (3.55)/(2.49)	0.034/0.057 (4.24)/(3.26)	$-0.027 \pm 0.013^{(b)}$
\mathcal{O}_{tt}	0.064/0.11 (3.00)/(2.32)	0.017/0.039 (5.87)/(3.85)	0.010/0.026 (7.46)/(4.70)	—
\mathcal{O}_{tb}	0.14/0.36 (2.33)/(1.46)	0.043/0.11 (4.24)/(2.64)	0.027/0.071 (5.30)/(3.30)	$-0.13 \pm 0.06^{(b)}$
\mathcal{O}_{t2}	0.010/0.023 (11.57)/(7.60)	0.0090/0.018 (12.18)/(8.62)	0.0089/0.017 (12.24)/(8.75)	$0.01^{(a)}$; $0.14 \pm 0.07^{(b)}$
\mathcal{O}_{Dt}	0.039/0.093 (2.84)/(1.85)	0.011/0.018 (5.27)/(4.15)	0.0052/0.0071 (7.84)/(6.68)	$0.03^{(a)}$; $-0.06 \pm 0.03^{(b)}$
$\mathcal{O}_{tW\Phi}$	0.0010/0.0021 (42.67)/(29.97)	0.00067/0.0010 (53.14)/(42.73)	0.00043/0.00056 (66.16)/(58.10)	$0.014^{(a)}$
$\mathcal{O}_{tB\Phi}$	0.0011/0.0027 (41.63)/(26.52)	0.00079/0.0015 (48.82)/(36.11)	0.00060/0.0012 (55.89)/(39.80)	$0.013^{(a)}$
$\mathcal{O}_{tG\Phi}$	0.027/0.029 (7.86)/(7.30)	0.023/0.025 (9.08)/(8.54)	0.045/0.047 (4.71)/(4.52)	—
\mathcal{O}_W	0.065/0.13 (1.37)/(0.95)	0.021/0.045 (2.38)/(1.65)	0.014/0.030 (2.95)/(2.02)	$0.1^{(c)}$
$\mathcal{O}_{W\Phi}$	0.11/0.22 (1.35)/(0.94)	0.036/0.075 (2.35)/(1.63)	0.023/0.050 (2.91)/(1.99)	$0.1^{(c)}$
$\mathcal{O}_{B\Phi}$	0.071/0.14 ((2.98)/(2.09)	0.020/0.043 (5.66)/(3.81)	0.012/0.028 (7.14)/(4.76)	$0.1^{(c)}$
\mathcal{O}_{WW}	0.28/0.56 (1.56)/(1.10)	0.29/0.45 (1.52)/(1.22)	0.51/0.66 (1.15)/(1.01)	$0.015^{(c)}$
\mathcal{O}_{BB}	0.32/0.78 (1.99)/(1.27)	0.37/0.69 (1.83)/(1.35)	0.77/1.53 (1.27)/(0.91)	$0.05^{(c)}$
$\mathcal{O}_{\Phi 2}$	0.57/0.68	0.68/0.81	1.74/2.08	$0.01^{(c)}$

Appendix A

We give here the explicit expressions of the coefficients determining the NP effects of each anomalous coupling on the various observables \mathcal{A}^i that we consider. These expressions are given in terms of $\bar{d}_j^{L,R}$ couplings defined through (15) by

$$\bar{d}_j^{L,R} = d_j^{L,R} - d_j^{L,R,SM} \quad , \quad (\text{A.1})$$

in the form

$$\delta\mathcal{A}^i = \sum_{j=1,3} [K_j^L \bar{d}_j^L + K_j^R \bar{d}_j^R] \quad . \quad (\text{A.2})$$

They are obtained from the expressions (29-42) of the observables and the expansions to first order in NP couplings of the combinations (24-28). Thus, using the definitions

$$a_1 \equiv A_{2SM}^{L+R} + \frac{2m_t^2}{s} A_{1SM}^{L+R} \quad , \quad a_2 = A_{2SM}^{L+R} - \frac{4m_t^2}{s} A_{1SM}^{L+R} \quad , \quad (\text{A.3})$$

$$b_1 = A_{2SM}^{L-R} + \frac{2m_t^2}{s} A_{1SM}^{L-R} \quad , \quad b_2 = A_{2SM}^{L-R} - \frac{4m_t^2}{s} A_{1SM}^{L-R} \quad , \quad (\text{A.4})$$

and the combinations $A_{iSM}^{L\pm R}$, $B_{iSM}^{L\pm R}$ and $C_{iSM}^{L\pm R}$ computed from (24-28) with

$$d_{1SM}^L = \frac{2}{3} + \frac{(1 - 2s_W^2)(1 - \frac{8}{3}s_W^2)}{8s_W^2 c_W^2} \chi \quad \quad d_{1SM}^R = \frac{2}{3} - \frac{1 - \frac{8}{3}s_W^2}{4c_W^2} \chi \quad (\text{A.5})$$

$$d_{2SM}^L = -\frac{1 - 2s_W^2}{8s_W^2 c_W^2} \chi \quad \quad d_{2SM}^R = \frac{\chi}{4c_W^2} \quad (\text{A.6})$$

we get

a) Integrated observables

σ_t

$$\begin{aligned} K_1^L &= \frac{2d_{1SM}^L}{a_1} \left(1 + \frac{2m_t^2}{s}\right) \quad , \quad K_1^R = \frac{2d_{1SM}^R}{a_1} \left(1 + \frac{2m_t^2}{s}\right) \quad , \\ K_2^L &= 2\beta_t^2 \frac{d_{2SM}^L}{a_1} \quad , \quad K_2^R = 2\beta_t^2 \frac{d_{2SM}^R}{a_1} \quad , \\ K_3^L &= -2\beta_t^2 \frac{d_{1SM}^L}{a_1} \quad , \quad K_3^R = -2\beta_t^2 \frac{d_{1SM}^R}{a_1} \quad , \end{aligned} \quad (\text{A.7})$$

H_t

$$\begin{aligned} K_1^L &= \frac{d_{2SM}^L}{B_{1SM}^{L+R}} , & K_1^R &= \frac{d_{2SM}^R}{B_{1SM}^{L+R}} , \\ K_2^L &= \frac{d_{1SM}^L}{B_{1SM}^{L+R}} , & K_2^R &= \frac{d_{1SM}^R}{B_{1SM}^{L+R}} , \end{aligned} \quad (\text{A.8})$$

T_t

$$\begin{aligned} K_1^L &= \frac{2d_{1SM}^L}{C_{1SM}^{L+R}} , & K_1^R &= -\frac{2d_{1SM}^R}{C_{1SM}^{L+R}} , \\ K_3^L &= -\left(\frac{2|\vec{p}|^2}{m_t^2}\right) \frac{d_{1SM}^L}{C_{1SM}^{L+R}} , & K_3^R &= \left(\frac{2|\vec{p}|^2}{m_t^2}\right) \frac{d_{1SM}^R}{C_{1SM}^{L+R}} , \end{aligned} \quad (\text{A.9})$$

b) Unpolarized asymmetries

A_{FB}

$$\begin{aligned} K_1^L &= \frac{d_{2SM}^L}{A_{3SM}^{L+R}} - \frac{2d_{1SM}^L(1 + \frac{2m_t^2}{s})}{a_1} , & K_1^R &= -\frac{d_{2SM}^R}{A_{3SM}^{L+R}} - \frac{2d_{1SM}^R(1 + \frac{2m_t^2}{s})}{a_1} , \\ K_2^L &= \frac{d_{1SM}^L}{A_{3SM}^{L+R}} - 2\beta_t^2 \frac{d_{2SM}^L}{a_1} , & K_2^R &= -\frac{d_{1SM}^R}{A_{3SM}^{L+R}} - 2\beta_t^2 \frac{d_{2SM}^R}{a_1} , \\ K_3^L &= 2\beta_t^2 \frac{d_{1SM}^L}{a_1} , & K_3^R &= 2\beta_t^2 \frac{d_{1SM}^R}{a_1} , \end{aligned} \quad (\text{A.10})$$

A_{EC}

$$\begin{aligned} K_1^L &= \frac{2d_{1SM}^L(1 - \frac{4m_t^2}{s}) - 2d_{1SM}^L(1 + \frac{2m_t^2}{s})}{a_2} , & K_2^L &= 2\beta_t^2 d_{2SM}^L \left(\frac{1}{a_2} - \frac{1}{a_1}\right) , \\ K_1^R &= \frac{2d_{1SM}^R(1 - \frac{4m_t^2}{s}) - 2d_{1SM}^R(1 + \frac{2m_t^2}{s})}{a_2} , & K_2^R &= 2\beta_t^2 d_{2SM}^R \left(\frac{1}{a_2} - \frac{1}{a_1}\right) , \\ K_3^L &= 4\beta_t^2 d_{1SM}^L \left(\frac{1}{a_2} + \frac{1}{2a_1}\right) , & K_3^R &= 4\beta_t^2 d_{1SM}^R \left(\frac{1}{a_2} + \frac{1}{2a_1}\right) , \end{aligned} \quad (\text{A.11})$$

H_{FB}

$$\begin{aligned} K_1^L &= \frac{2d_{1SM}^L}{B_{2SM}^{L+R}} - \frac{d_{2SM}^L}{B_{1SM}^{L+R}} , & K_1^R &= -\frac{2d_{1SM}^R}{B_{2SM}^{L+R}} - \frac{d_{2SM}^R}{B_{1SM}^{L+R}} , \\ K_2^L &= 2\beta_t^2 \frac{d_{2SM}^L}{B_{2SM}^{L+R}} - \frac{d_{1SM}^L}{B_{1SM}^{L+R}} , & K_2^R &= -2\beta_t^2 \frac{d_{2SM}^R}{B_{2SM}^{L+R}} - \frac{d_{1SM}^R}{B_{1SM}^{L+R}} , \end{aligned} \quad (\text{A.12})$$

T_{FB}

$$\begin{aligned}
K_1^L &= \frac{d_{2SM}^L}{C_{2SM}^{L+R}} - \frac{2d_{1SM}^L}{C_{1SM}^{L+R}} , & K_1^R &= \frac{d_{2SM}^R}{C_{2SM}^{L+R}} + \frac{2d_{1SM}^R}{C_{1SM}^{L+R}} , \\
K_2^L &= \frac{d_{1SM}^L}{C_{2SM}^{L+R}} , & K_2^R &= \frac{d_{1SM}^R}{C_{2SM}^{L+R}} , \\
K_3^L &= -\frac{2|\vec{p}|^2}{m_t^2} \left[\frac{d_{2SM}^L}{C_{2SM}^{L+R}} - \frac{d_{1SM}^L}{C_1^{L+R}} \right] , & K_3^R &= -\frac{2|\vec{p}|^2}{m_t^2} \left[\frac{d_{2SM}^R}{C_{2SM}^{L+R}} + \frac{d_{1SM}^R}{C_1^{L+R}} \right] ,
\end{aligned} \tag{A.13}$$

c) Polarized asymmetries

A_{LR}

$$\begin{aligned}
K_1^L &= 2d_{1SM}^L \left(1 + \frac{2m_t^2}{s}\right) \left(\frac{1}{b_1} - \frac{1}{a_1}\right) , & K_1^R &= -2d_{1SM}^R \left(1 + \frac{2m_t^2}{s}\right) \left(\frac{1}{b_1} + \frac{1}{a_1}\right) , \\
K_2^L &= 2\beta_t^2 d_{2SM}^L \left(\frac{1}{b_1} - \frac{1}{a_1}\right) , & K_2^R &= -2\beta_t^2 d_{2SM}^R \left(\frac{1}{b_1} + \frac{1}{a_1}\right) , \\
K_3^L &= -2\beta_t^2 d_{1SM}^L \left(\frac{1}{b_1} - \frac{1}{a_1}\right) , & K_3^R &= 2\beta_t^2 d_{1SM}^R \left(\frac{1}{b_1} + \frac{1}{a_1}\right) ,
\end{aligned} \tag{A.14}$$

$A_{FB}^{(pol)}$

$$\begin{aligned}
K_1^L &= \frac{d_{2SM}^L}{A_{3SM}^{L-R}} - \frac{2d_{1SM}^L}{b_1} \left(1 + \frac{2m_t^2}{s}\right) , & K_1^R &= \frac{d_{2SM}^R}{A_{3SM}^{L-R}} + \frac{2d_{1SM}^R}{b_1} \left(1 + \frac{2m_t^2}{s}\right) , \\
K_2^L &= \frac{d_{1SM}^L}{A_{3SM}^{L-R}} - 2\beta_t^2 \frac{d_{2SM}^L}{b_1} , & K_2^R &= \frac{d_{1SM}^R}{A_{3SM}^{L-R}} + 2\beta_t^2 \frac{d_{2SM}^R}{b_1} , \\
K_3^L &= 2\beta_t^2 \frac{d_{1SM}^L}{b_1} , & K_3^R &= -2\beta_t^2 \frac{d_{1SM}^R}{b_1} ,
\end{aligned} \tag{A.15}$$

$A_{EC}^{(pol)}$

$$\begin{aligned}
K_1^L &= \frac{2d_{1SM}^L}{b_2} \left(1 - \frac{4m_t^2}{s}\right) - \frac{2d_{1SM}^L}{b_1} \left(1 + \frac{2m_t^2}{s}\right) , & K_2^L &= 2\beta_t^2 d_{2SM}^L \left(\frac{1}{b_2} - \frac{1}{b_1}\right) , \\
K_1^R &= -\frac{2d_{1SM}^R}{b_2} \left(1 - \frac{4m_t^2}{s}\right) + \frac{2d_{1SM}^R}{b_1} \left(1 + \frac{2m_t^2}{s}\right) , & K_2^R &= -2\beta_t^2 d_{2SM}^R \left(\frac{1}{b_2} - \frac{1}{b_1}\right) , \\
K_3^L &= 4\beta_t^2 d_{1SM}^L \left(\frac{1}{b_2} + \frac{1}{2b_1}\right) , & K_3^R &= -4\beta_t^2 d_{1SM}^R \left(\frac{1}{b_2} + \frac{1}{2b_1}\right) ,
\end{aligned} \tag{A.16}$$

H_{LR}

$$\begin{aligned} K_1^L &= d_{2SM}^L \left(\frac{1}{A_{3SM}^{L+R}} - \frac{1}{A_{3SM}^{L-R}} \right) , & K_1^R &= -d_{2SM}^R \left(\frac{1}{A_{3SM}^{L+R}} + \frac{1}{A_{3SM}^{L-R}} \right) , \\ K_2^L &= d_{1SM}^L \left(\frac{1}{A_{3SM}^{L+R}} - \frac{1}{A_{3SM}^{L-R}} \right) , & K_2^R &= -d_{1SM}^R \left(\frac{1}{A_{3SM}^{L+R}} + \frac{1}{A_{3SM}^{L-R}} \right) , \end{aligned} \quad (\text{A.17})$$

$H_{FB}^{(pol)}$

$$\begin{aligned} K_1^L &= \frac{2d_{1SM}^L}{A_{2SM}^{L+R}} - \frac{d_{2SM}^L}{A_{3SM}^{L+R}} , & K_1^R &= \frac{2d_{1SM}^R}{A_{2SM}^{L+R}} + \frac{d_{2SM}^R}{A_{3SM}^{L+R}} , \\ K_2^L &= \frac{2\beta_t^2 d_{2SM}^L}{A_{2SM}^{L+R}} - \frac{d_{1SM}^L}{A_{3SM}^{L+R}} , & K_2^R &= \frac{2\beta_t^2 d_{2SM}^R}{A_{2SM}^{L+R}} + \frac{d_{1SM}^R}{A_{3SM}^{L+R}} , \end{aligned} \quad (\text{A.18})$$

T_{LR}

$$\begin{aligned} K_1^L &= 2d_{1SM}^L \left(\frac{1}{C_{1SM}^{L-R}} - \frac{1}{C_{1SM}^{L+R}} \right) , & K_3^L &= - \left(\frac{2|\vec{p}|^2}{m_t^2} \right) d_{1SM}^L \left(\frac{1}{C_{1SM}^{L-R}} - \frac{1}{C_{1SM}^{L+R}} \right) , \\ K_1^R &= 2d_{1SM}^R \left(\frac{1}{C_{1SM}^{L-R}} + \frac{1}{C_{1SM}^{L+R}} \right) , & K_3^R &= - \left(\frac{2|\vec{p}|^2}{m_t^2} \right) d_{1SM}^R \left(\frac{1}{C_{1SM}^{L-R}} + \frac{1}{C_{1SM}^{L+R}} \right) , \end{aligned} \quad (\text{A.19})$$

$T_{FB}^{(pol)}$

$$\begin{aligned} K_1^L &= \frac{d_{2SM}^L}{C_{2SM}^{L-R}} - \frac{2d_{1SM}^L}{C_{1SM}^{L-R}} , & K_1^R &= -\frac{d_{2SM}^R}{C_{2SM}^{L-R}} - \frac{2d_{1SM}^R}{C_{1SM}^{L-R}} , \\ K_2^L &= \frac{d_{1SM}^L}{C_{2SM}^{L-R}} , & K_2^R &= -\frac{d_{1SM}^R}{C_{2SM}^{L-R}} , \\ K_3^L &= -\frac{2|\vec{p}|^2}{m_t^2} \left(\frac{d_{2SM}^L}{C_{2SM}^{L-R}} - \frac{d_{1SM}^L}{C_{1SM}^{L-R}} \right) , & K_3^R &= \frac{2|\vec{p}|^2}{m_t^2} \left(\frac{d_{2SM}^R}{C_{2SM}^{L-R}} + \frac{d_{1SM}^R}{C_{1SM}^{L-R}} \right) . \end{aligned} \quad (\text{A.20})$$

The coefficients for the \bar{d}_j^γ and \bar{d}_j^Z couplings are easily obtained from relations (15).

$$K_j^\gamma = K_j^L + K_j^R \quad K_j^Z = \frac{1 - 2s_W^2}{4s_W^2 c_W^2} \chi K_j^L - \frac{\chi}{2c_W^2} K_j^R \quad (\text{A.21})$$

This allows to write:

$$\delta\mathcal{A}^i = \sum_{j=1,3} [K_j^\gamma \bar{d}_j^\gamma + K_j^Z \bar{d}_j^Z] . \quad (\text{A.22})$$

In Table A1 we give for illustration the values of these $K_j^{\gamma,Z}$ coefficients at 1 TeV. With this table one can appreciate the role of each observable, non polarized asymmetry, polarized asymmetry and integrated ρ elements (taken with a 2% normalization uncertainty), in establishing the limits for each coupling.

Table A1: Numerical values of $K_j^{\gamma,Z}$ at 1 TeV.

\mathcal{A}^i	d_1^γ	d_2^γ	d_3^γ	d_1^Z	d_2^Z	d_3^Z
A_{FB}	-28.98	-15.86	63.50	-9.74	-42.37	12.17
A_{EC}	-0.68	-0.10	52.07	-0.13	-0.95	9.98
H_{FB}	-5.14	-39.36	0.00	-5.62	-9.01	0.00
T_{FB}	-0.50	-4.81	2.23	-0.68	-0.92	-7.76
$A_{LR}^{(A)}$	-17.51	-51.63	14.47	79.91	7.24	-66.07
$A_{FB}^{(pol)}$	-8.42	-65.45	9.86	-9.33	-14.80	35.38
$A_{EC}^{(pol)}$	-0.06	-1.51	10.28	-0.21	-0.16	36.89
$A_{LR}^{(B)}$	-5.26	-49.29	0.00	18.34	0.00	0.00
$H_{FB}^{(pol)}$	-15.61	-8.73	0.00	-5.31	-22.85	0.00
$A_{LR}^{(C)}$	4.38	0.00	-31.39	-15.27	0.00	109.39
$T_{FB}^{(pol)}$	-2.44	-0.98	-0.88	-0.69	-3.52	3.05
σ_t	82.36	-2.62	-68.10	15.78	-24.98	-13.05
H_t	2.13	-55.49	0.00	20.35	-10.63	0.00
T_t	5.06	0.00	-36.26	18.16	0.00	-130.11

References

- [1] S.J. Wimpenny and B.L. Winer, Nevis-1525, UCR/d0/96-14, CDF/PUB/TOP/PUBLIC/3681, D0 Note 2957 (1996).
- [2] For a review, see e.g., J.H. Kühn, TTP96-18 (1996); F. Larios, E. Malkawi and C.-P. Yuan, MSUHEP-60922, hep-ph/9609482; D.O. Carlson and C.-P. Yuan, MSUHEP-50823, 1995; C.-P. Yuan hep-ph/9604434.
- [3] P.B. Renton, Rapporteur talk at the Int. Conf. on High Energy Physics, Beijing (1995); P. Langacker, NSF-ITP-95-140, UPR-0683T, Oct. 95; D.G. Charlton, talk at the Int. EPS-HEP Conf. Brussels 1995, PA 8/1-6; K. Hagiwara, talk at the Int. Conf. on High Energy Physics, Beijing (1995), KEK-TH-461; P.S. Wells, talk at CERN. For the most recent situation see the talks of A. Blondel and M.W. Grunewald at the Warsaw conference on High Energy Physics (1996).
- [4] W. Buchmüller and D. Wyler, Nucl. Phys. **B268** (1986) 621; C.J.C. Burgess and H.J. Schnitzer, Nucl. Phys. **B228** (1983) 454; C.N. Leung, S.T. Love and S. Rao Z. Phys. **C31** (1986) 433.
- [5] G.J. Gounaris, F.M. Renard and C. Verzegnassi, Phys. Rev. **D52** (1995) 451.
- [6] G.J. Gounaris, M. Kuroda and F.M. Renard, PM/96-22, THES-TP 96/06, to appear in Phys. Rev. D.
- [7] G.J. Gounaris, D. Papadamou and F.M. Renard, PM/96-28, THES-TP 96/09, hep-ph/9609437.
- [8] E. Malkawi and C.-P. Yuan, Phys. Rev. **D52** (1995) 472. F. Larios and C.-P. Yuan, hep-ph/9606397.
- [9] C. Arzt, M.B. Einhorn and J. Wudka, Nucl. Phys. **B433** (1995) 41.
- [10] G.J. Gounaris, D. Papadamou and F.M. Renard, PM/96-31, THES-TP 96/10, hep-ph/9611224.
- [11] G.J. Gounaris, F.M. Renard and G. Tsirigoti, Phys. Lett. **B338** ((1994)) 51, Phys. Lett. **B350** ((1995)) 212.
- [12] e^+e^- Collisions at 500 GeV: The Physics Potential, Proceedings of the Workshop-Munich, Annecy, Hamburg, DESY 92-123A (1992), 92-123B (1992), 93-123C (1993), P.M. Zerwas ed.
- [13] R. Frey, talk given at Conf. on Phys. and Exp. with Linear Colliders, Morioka-Appi, Japan (1995), OREXP 96-04.
- [14] M. Hosch, K. Whisnant and B-L. Young, AMES-HET-96-04 (1996).

- [15] D. Chang, W-Y. Keung and I. Phillips, Nucl. Phys. **B408** (1993) 286.
- [16] P. Langacker, talk presented at *SUSY* – 95, Palaiseau, France, May 1995, U. of Pennsylvania report UPR-0683T.

Figure captions

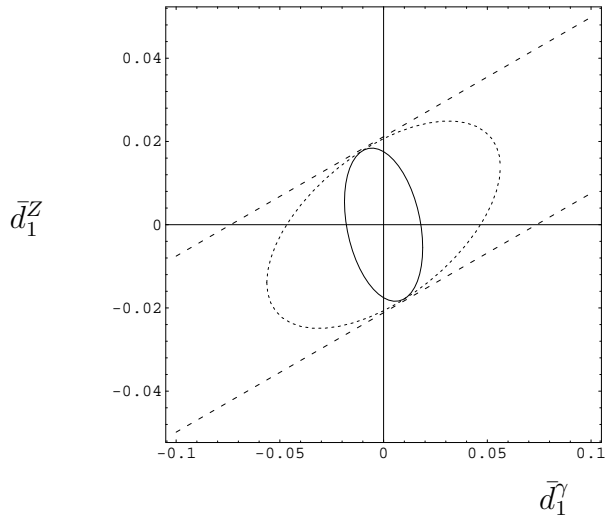
Fig.1 Observability limits in the 6-parameter case; with polarized beams (a) (c) (e) (g) (i) (k), with unpolarized beams (b) (d) (f) (h) (j) (l); from asymmetries alone (---), from asymmetries and σ_t, H_t, T_t with a normalization uncertainty of 2% (.....), 20% (———).

Fig.2 Observability limits in the 4-parameter case; same captions as in Fig.1.

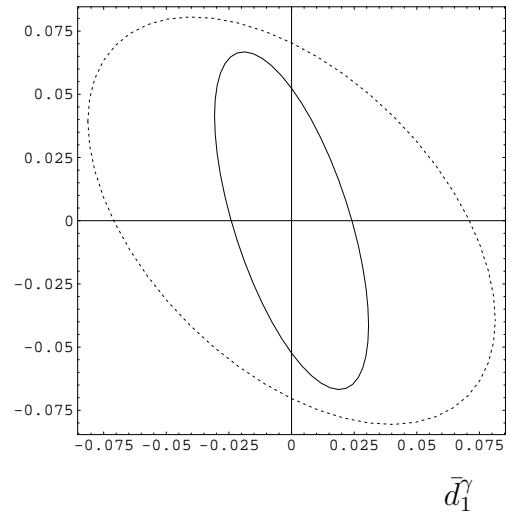
Fig.3 The observability ellipsoid in the 3-parameter case with polarized beams.

Fig.4 Observability limits in the 3-parameter case; with polarized beams (a)(c)(e), with unpolarized beams (b)(d)(f); same captions.

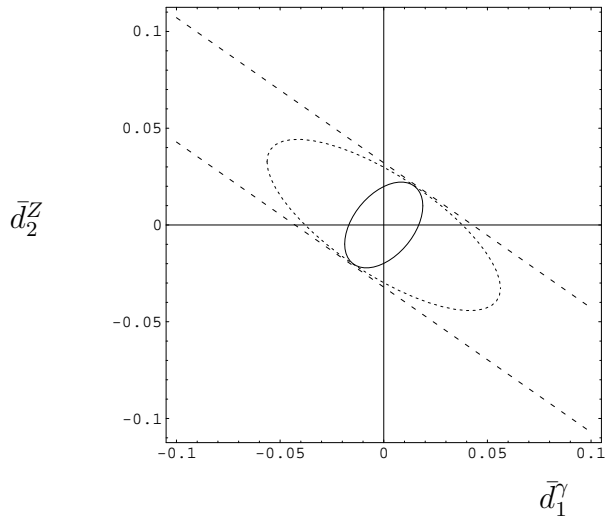
Fig.5 Observability limits in the 2-parameter case; with polarized beams (a), with unpolarized beams (b); same captions.



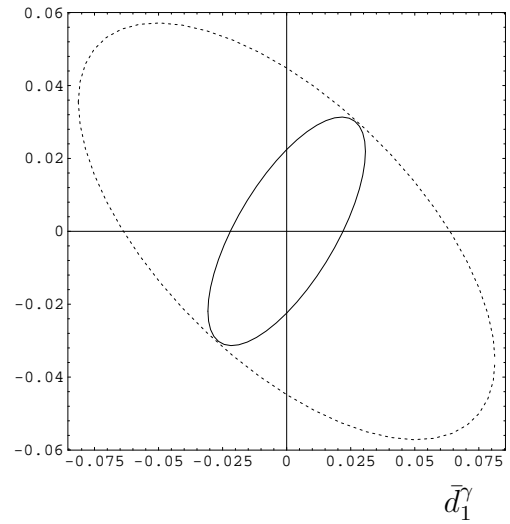
(a)



(b)



(c)



(d)

Fig 1

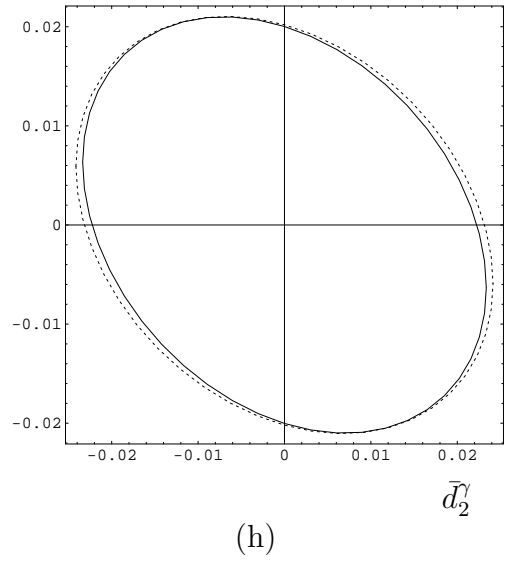
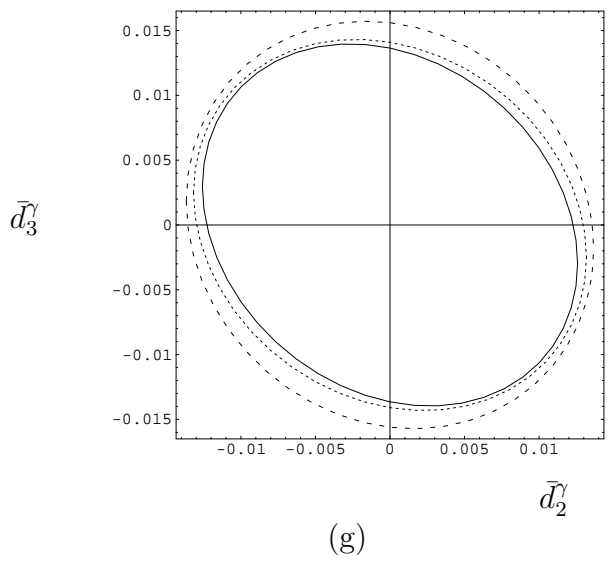
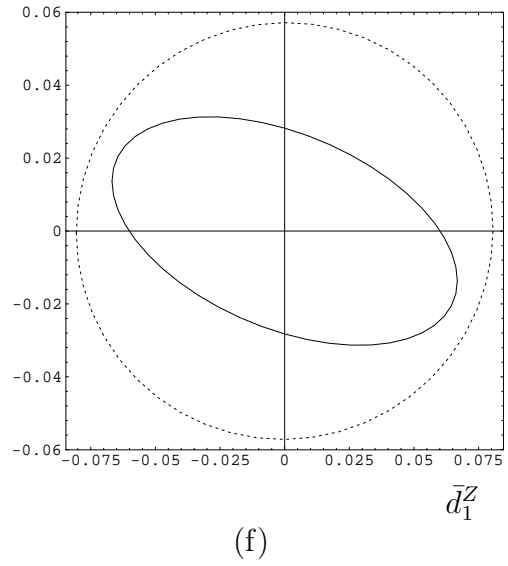
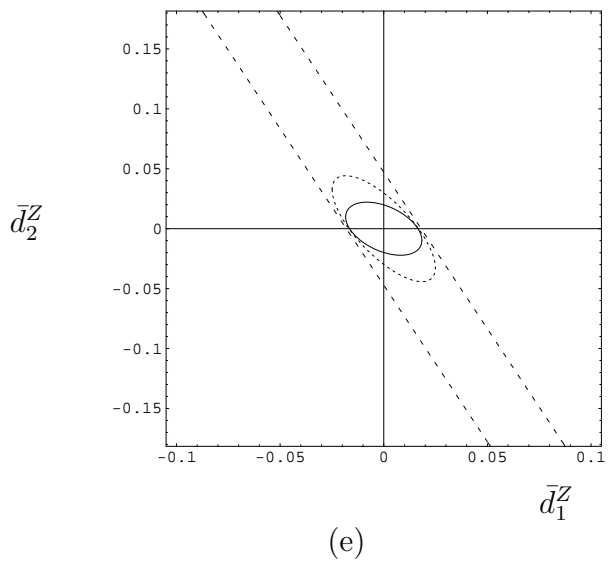
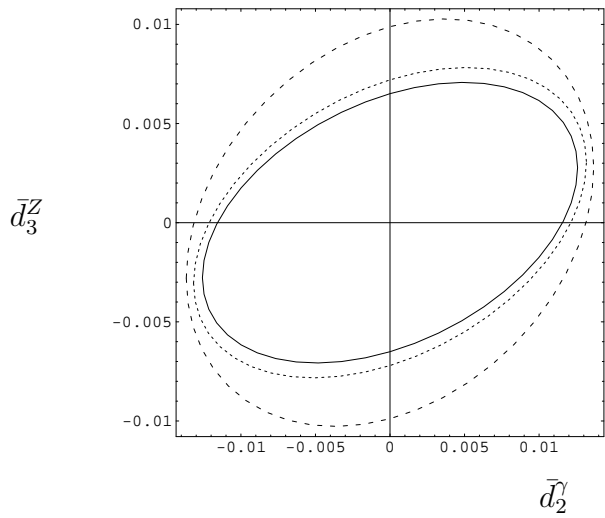
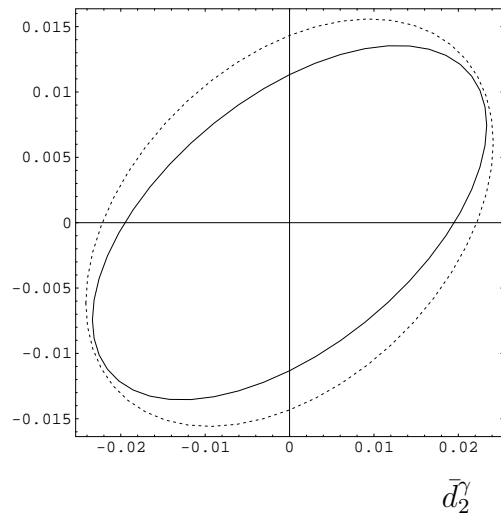


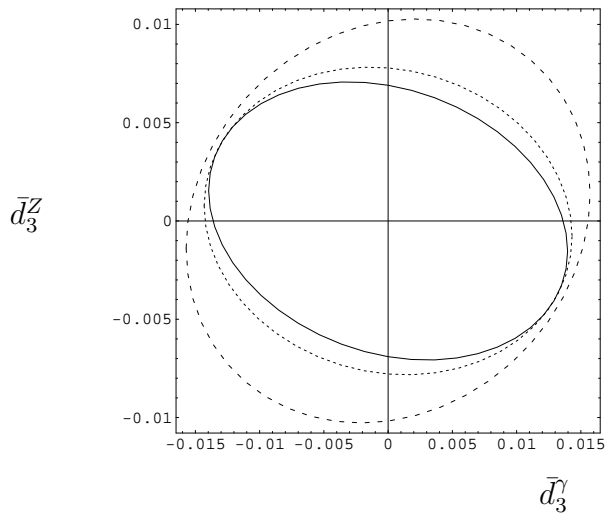
Fig 1



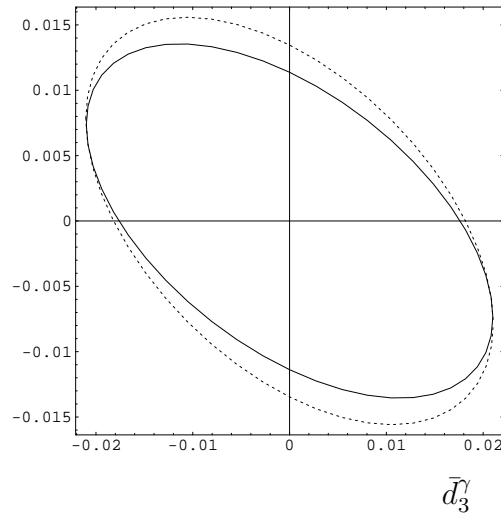
(i)



(j)



(k)



(l)

Fig 1

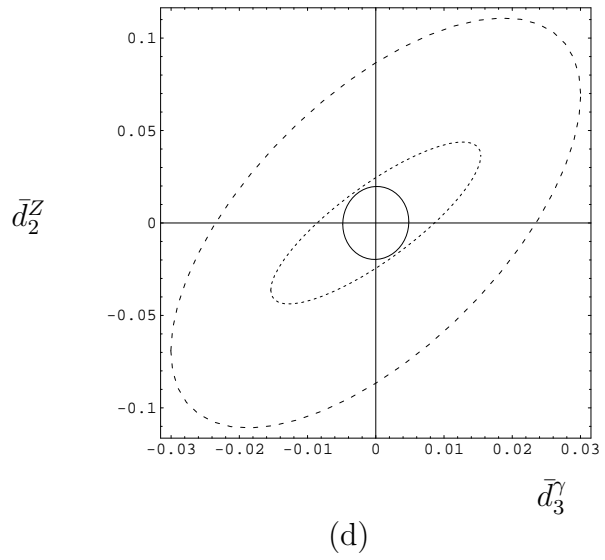
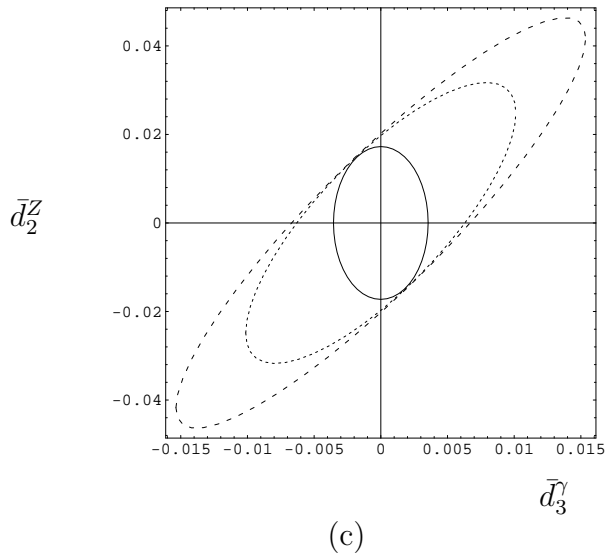
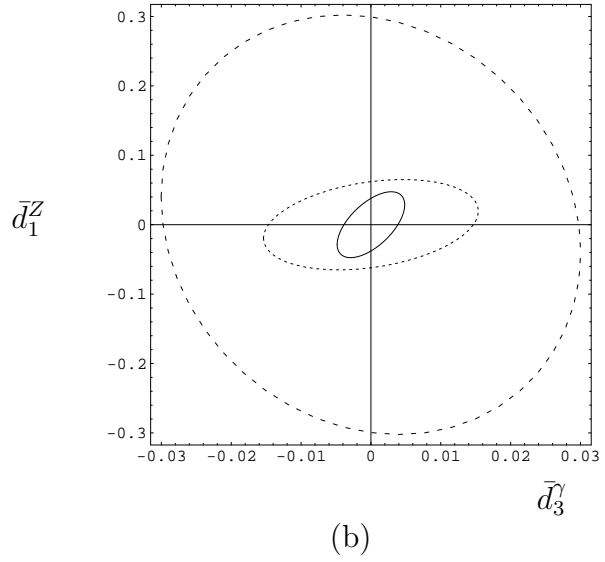
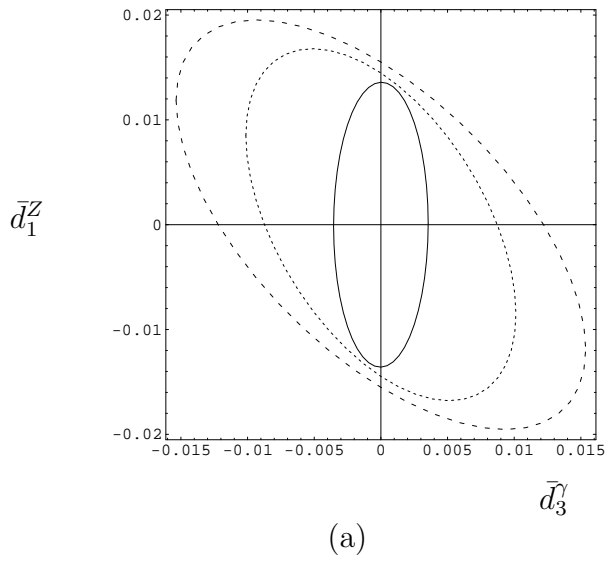


Fig 2

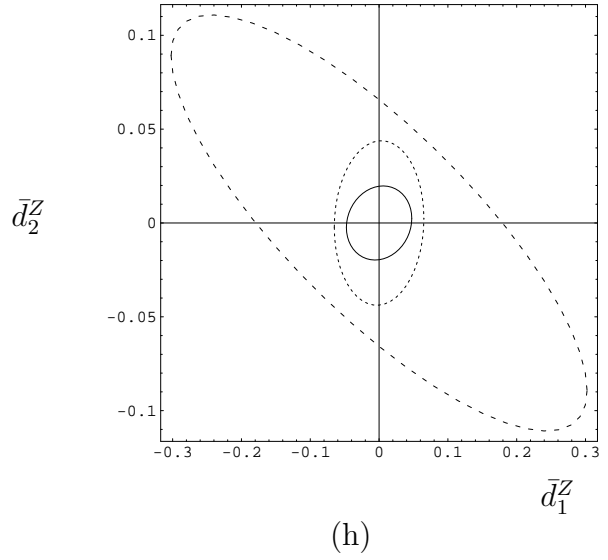
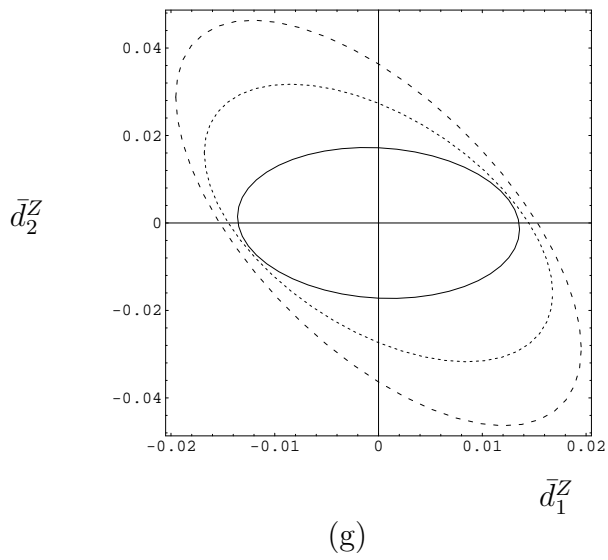
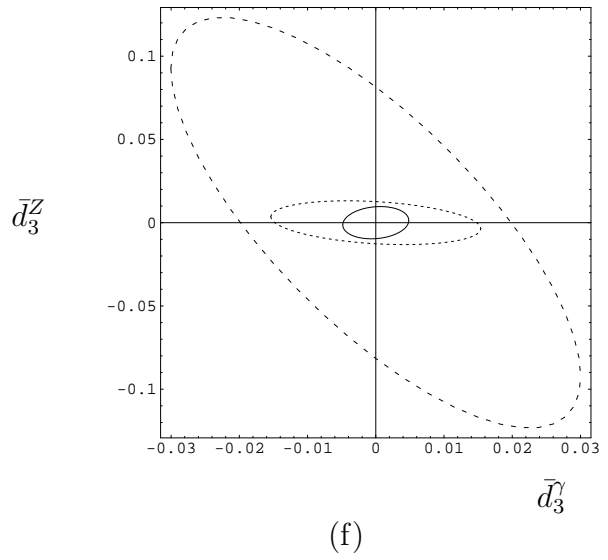
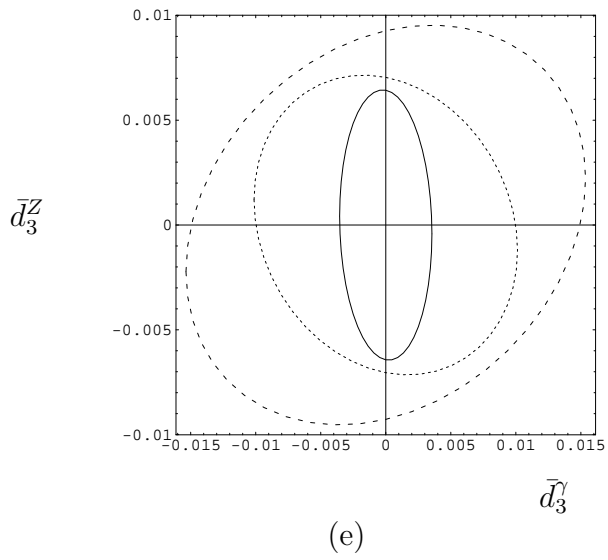


Fig 2

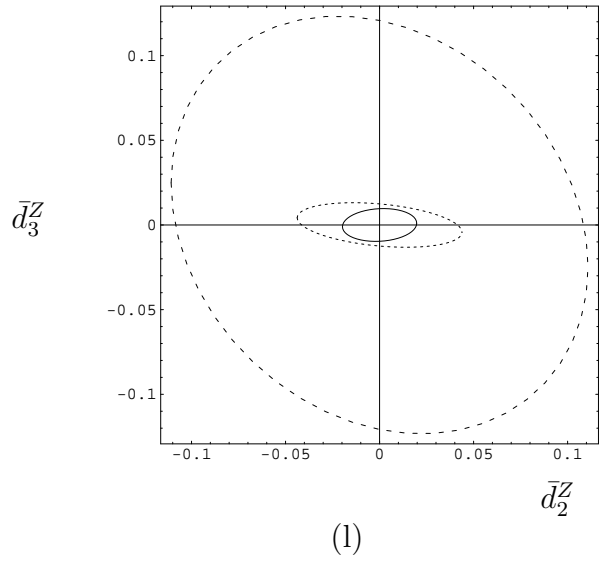
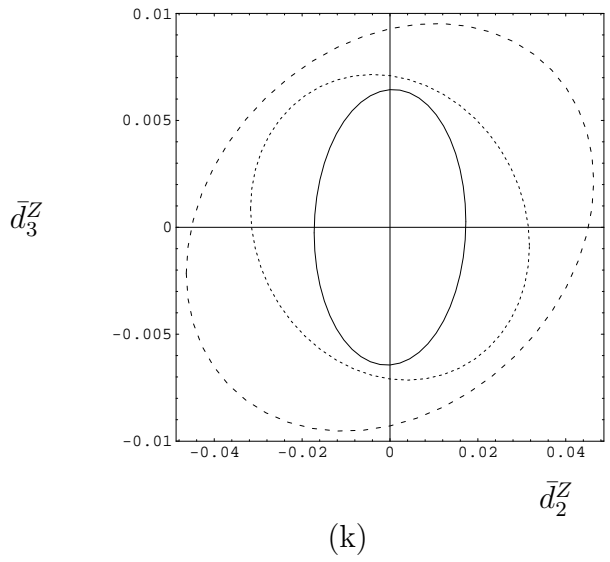
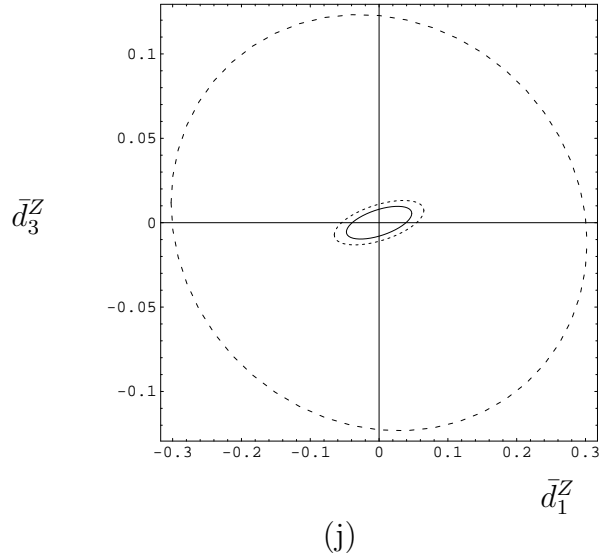
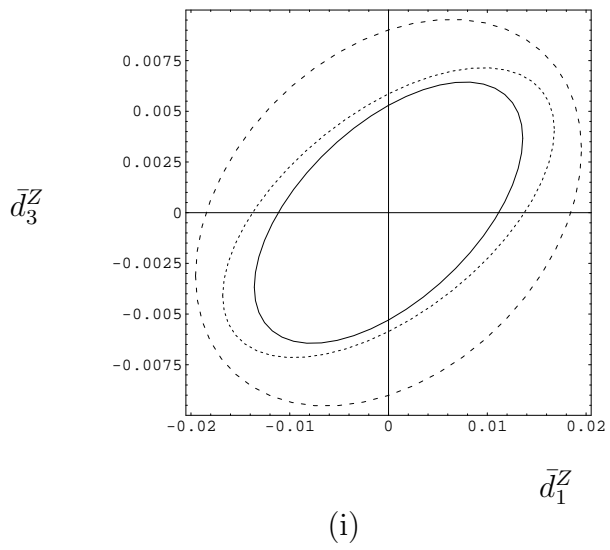


Fig 2

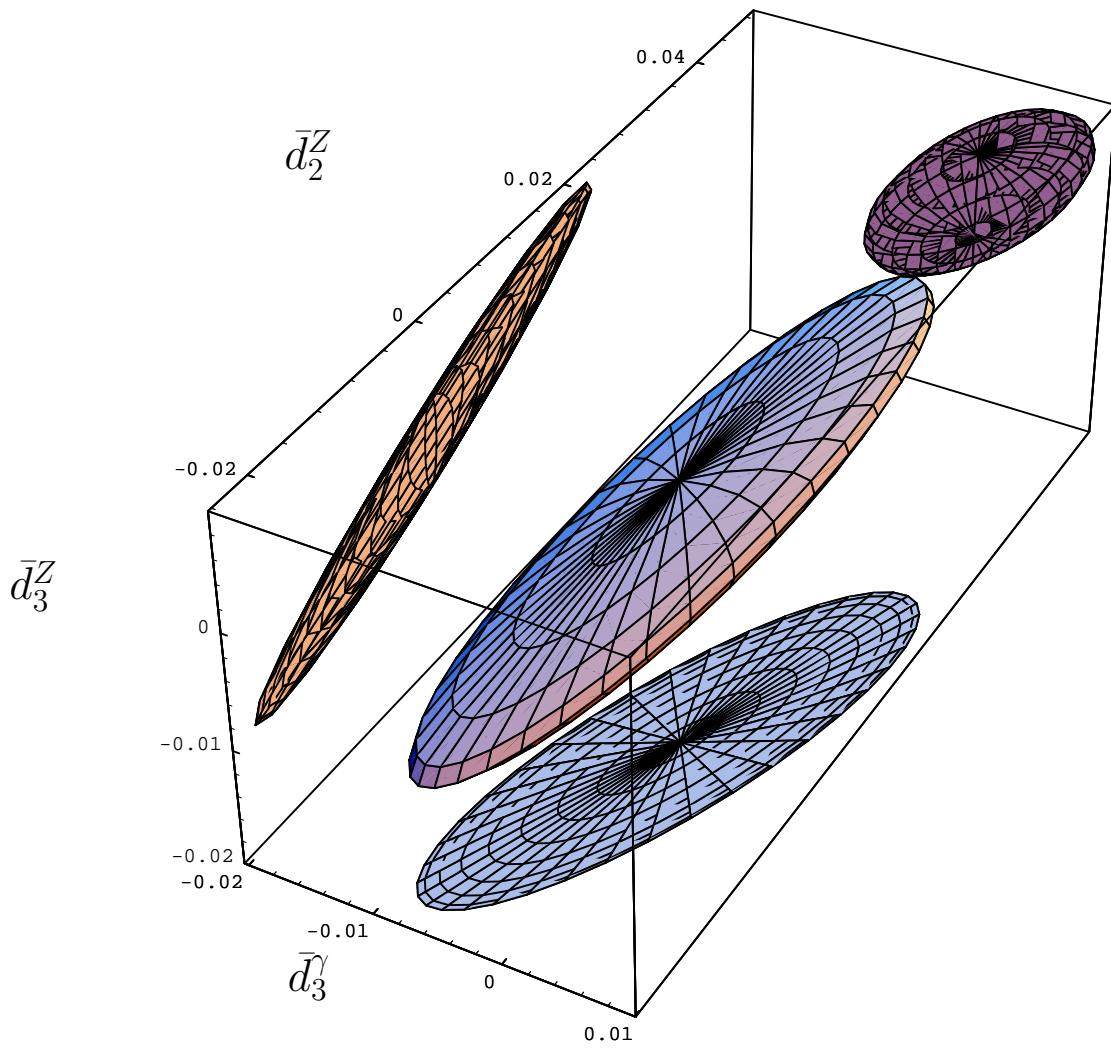
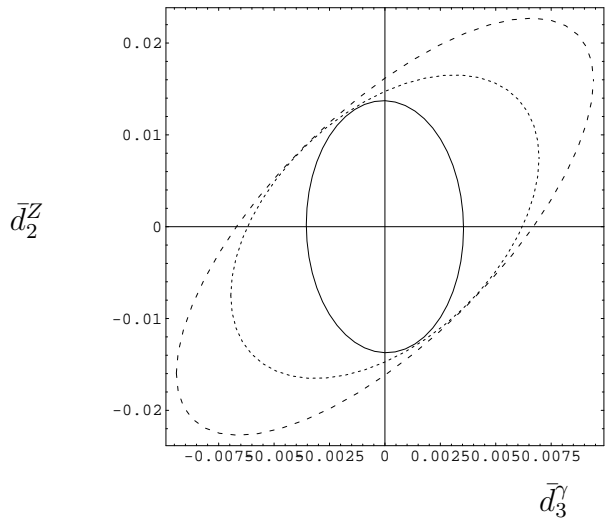
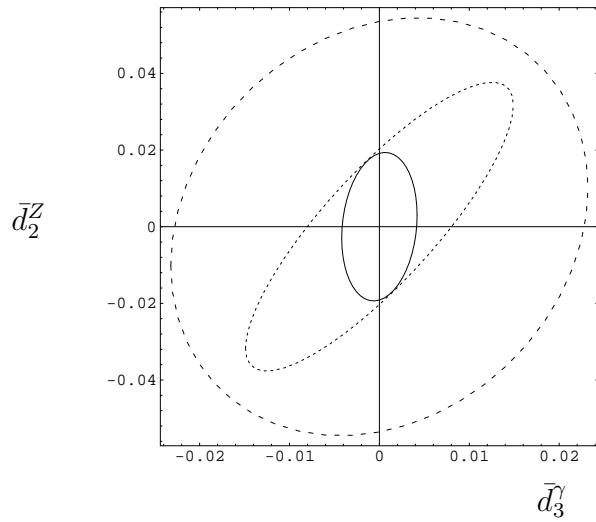


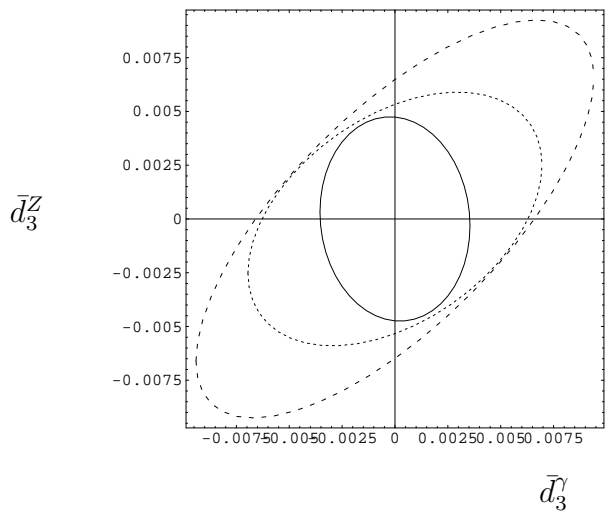
Fig 3



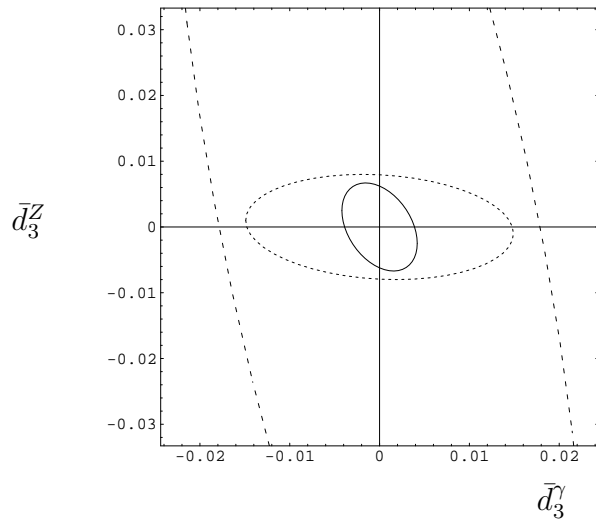
(a)



(b)

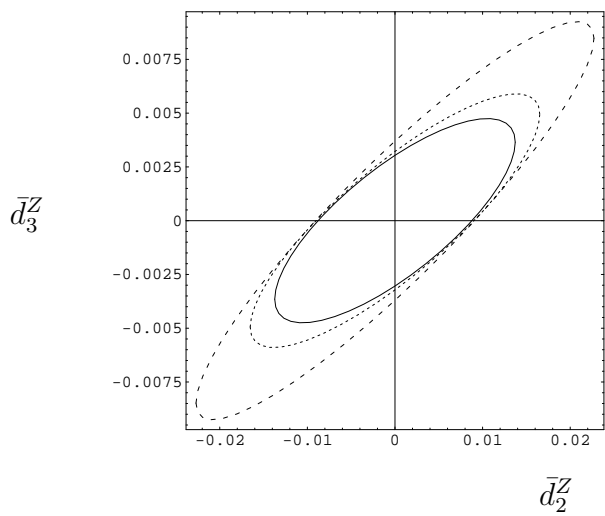


(c)

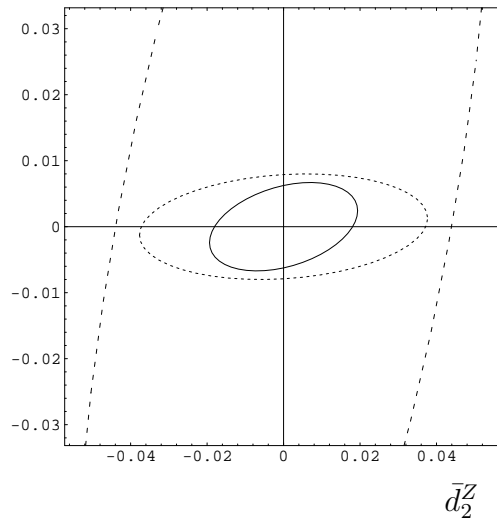


(d)

Fig 4

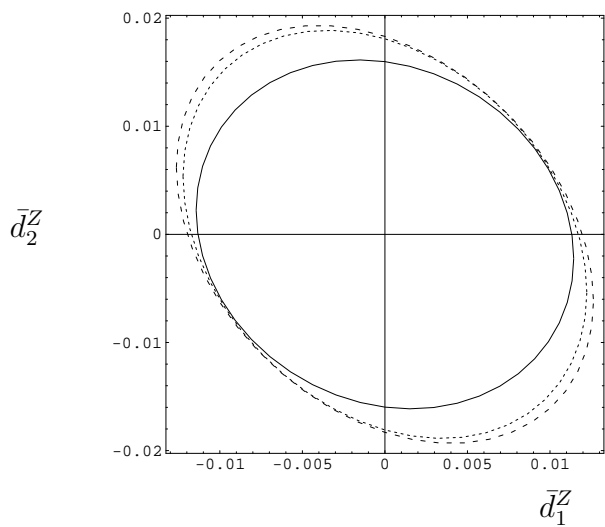


(e)

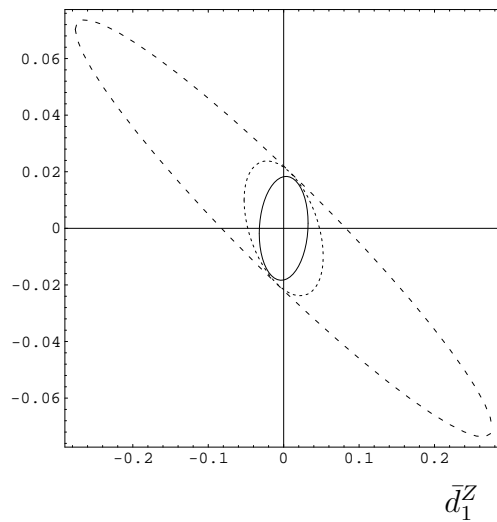


(f)

Fig 4



(a)



(b)

Fig 5